

BASIC METALLURGY OF MODERN NIOBIUM STEELS

Anthony J. DeArdo, Mingjian Hua and Calixto I. Garcia

Basic Metals Processing Research Institute
Department of Materials Science and Engineering
University of Pittsburgh, Pittsburgh, PA 15261, U.S.A.

Keywords: HSLA Steel, Nb, Thermomechanical Processing, Microalloying

Abstract

It is well known that niobium is added to a wide range of steels for improving processing, microstructure, properties and performance. Over the last two decades, the use of Nb has also permitted new steels with attractive properties to be developed. Furthermore, the addition of Nb to existing steels such as ferritic stainless and IF steels has also led to improvement. The goal of this paper is to review the basic behavior of niobium in a wide range of steels, including both the traditional steels and also some of the newer versions. Particular emphasis has been placed on the basic metallurgical principles that apply to these steels, for it is the application of these principles that allows the composition - processing - microstructure - mechanical property relationships to be rationalized and exploited. The application of basic metallurgical principles has resulted in a predictive capability that has led to alterations in composition and processing for the purpose of producing steels with superior mechanical properties and improved overall performance.

Introduction and History

As we celebrated in 2001 the 200th anniversary of the discovery of niobium by Charles Hatchett, we were reminded repeatedly of how this metal has changed the face of science and technology in the materials industry [1,2]. Nowhere is this more noticeable than in the case of steels. Although niobium is classified as a transition metal, perhaps the most important transition made by niobium was from being little more than a laboratory curiosity prior to 1960 to becoming a viable, commercially produced ferroalloy suitable for addition to steel in 1965. While we recognize 1801 as the date of the discovery of niobium, in fact, the first successful commercial production of ferroniobium at the Companhia Brasileira de Metalurgia e Mineração (CBMM) mine in Araxa, Brazil took place in 1965 [3]. After 1965, ferroniobium was abundantly available to the steel industry for the first time as a microalloying element. Prior to this date, only vanadium and titanium were available on a commercial scale for microalloying steel.

The 41st element in the periodic table is called columbium within the industrial sector of the USA and niobium by the rest of the world. The story behind the dual-names is quite interesting. John Winthrop (1609-1676), the first governor of Connecticut and a scientist and rock collector, discovered a new mineral around 1734. He named it columbite, possibly in honor of Christopher Columbus. Winthrop's grandson sent it to the British Museum for display and analysis in 1753. Decades later, in 1801, Charles Hatchett (1765-1847), a British chemist working at the British Museum, attempted to analyze the constitution of the columbite ore. Hatchett could tell that there was an element unknown at that time

present in the columbite, which he called columbium. In fact, unbeknownst to Hatchett, there were two then unknown elements in the columbite: columbium and tantalum. In 1802, the Swedish chemist A.G. Ekeberg discovered a new element in Finnish minerals similar to columbite and named it tantalum after the Greek god Tantalus. The situation became confused when in 1809, the British chemist and physicist, William Hyde Wollaston, compared the minerals tantalite and columbite and declared that the element columbium was actually the element tantalum. This confusion was not unexpected since the elements are so similar, are always found together in natural deposits, and are very difficult to separate. In 1844, Heinrich Rose, a German chemist, produced two apparently new and different acids from columbite and tantalite. One came to be known as niobic acid, while the other was called tantalic or pelopic acid. Rose found that the element contained within the tantalic acid was very similar to tantalum described by Ekeberg, hence the name tantalic acid. The undefined element found in the other acid was called niobium, hence the name niobic acid, after Niobe, mythical daughter of Tantalus and goddess of tears. About twenty years later, the Swiss chemist Jean Charles Galissard de Marignac proved that these two acids were both distinct and produced by two different elements. Finally, the Swedish chemist Christian Wilhelm Blomstrand isolated metallic niobium in 1864. The name niobium was officially adopted by the International Union of Pure and Applied Chemistry in 1950, although the metal is still referred to as columbium, especially in the industrial metallurgical sector of the USA. The two names will be used interchangeably in this paper.

Although the benefits of niobium additions to low carbon steel were known since the late 1930's [4], it was not until 1958 that the first heat of niobium microalloyed steel in the form of hot strip was commercially produced by National Steel in the United States [5]. The international symposium, *Niobium*, held in San Francisco in 1981, reviewed the science and technology of using niobium in a broad range of materials as practiced at that time [6]. By 1981, the concepts of controlled rolling, austenite conditioning, and proper alloy design for ferrite-pearlite microstructures with adequate properties in a broad range of products were understood and practiced.

Perhaps the plate and linepipe microalloyed steels were the best understood and optimized at that time. On the other hand, the benefits of niobium microalloying to product lines such as strip, sheet, bars, shapes and castings were just starting to be exploited. Most of the work published in the steel papers in *Niobium* concerned ferrite-pearlite microstructures [6].

What has changed since 1981 concerning the benefits of Nb microalloying to steels? There have been at least two major changes in the Nb bearing steel products over the past 20 years. First, since polygonal ferrite-pearlite microstructures cannot readily exceed yield strength levels of about 400 MPa in reasonable section sizes and low carbon contents found in Nb steels, the applications-driven requirement for higher strength levels has led to the development of ferritic microstructures in virtually every product class that are based on low temperature transformation products such as acicular ferrite and bainite or multiphase microstructures. Sometimes these microstructures are achieved through the use of accelerated cooling, sometimes by using hardenability approaches, or sometimes additions of Nb improve both. Regardless of the approach, Nb continues to play a major positive role in optimizing the manufacturability, final properties and performance of these steels.

The second major change since 1981 has been in the wide acceptance of Nb as a stabilizing element, often in combination with Ti, whereby carbides are formed thus reducing the amount of free carbon in solid solution, in both ultra-low carbon sheet steel (ULC) and ferritic stainless steel. Since the Nb levels employed in the ULC steels frequently fall in the range 100-300 ppm, they can be considered as a microalloying addition. However, the 1500-5000 ppm Nb sometimes used in the ferritic stainless steels would be considered an alloying addition. The so-called dual-stabilized Ti + Nb containing ULC steels

and ferritic stainless steels are viable, successful, and growing members of their respective families.

The forerunner of this current paper appeared in the Proceedings of *Niobium* [7]. In that paper, the authors attempted to present the fundamental aspects of Nb and its behavior in steel as understood at that time. These fundamental aspects have remained valid over the course of time. However, much has been learned in the intervening 20 years that will expand upon what was presented in the earlier paper. This current paper will be organized as follows:

- A. Introduction and History
- B. Solubility Products and Precipitation in Austenite
- C. Thermomechanical Processing and Austenite Conditioning in Nb Steel
- D. Transformation and Strengthening in Nb Steels
- E. Niobium and Stabilization

The goal of this paper is to provide the reader with the background necessary to understand modern Nb microalloyed steels. The basic principles presented here will hopefully permit the reader to design better steels and processing routes to further improve future steels, all through the intelligent use of Nb. The application side is becoming even more demanding: weight reduction, safety, lower cost, etc. These increasing demands can only be met through a thorough understanding of the literature and of the basic principles of microalloying with Nb upon which much progress depends. A more complete version of this paper is available [8].

Solubility Products and Precipitation in Austenite

Microalloyed steels contain both carbon and nitrogen and when niobium precipitates it does so as niobium carbonitride [9-13]. The crystallography of “NbC” has been discussed above and, in fact, is very similar to “NbN” [14]. Since “NbC” and “NbN” are very similar compounds, it is quite reasonable to expect the two to have complete solid solubility, i.e. form a carbonitride. This is, in fact, correct [15].

The NbC-NbN system has been studied [16,17] and reviewed [18]. The NbC-NbN system is actually a ternary system of NbC, NbN and vacancies. This ternary system and associated lattice parameters are shown in Figure 1. Two very important points emerge from an inspection of Figure 1. First, the composition of niobium carbonitride can be represented by NbC_xN_y where x equals the mole ratio of C/Nb, y equals the mole ratio of N/Nb and $1 - (x + y)$ equals the mole ratio of vacancies. Figure 1 also indicates that the quantities x , y and $(x + y)$ can all be variables. Second, the lattice parameters of the carbonitride will be strongly influenced by both the nitrogen and vacancy concentration; both nitrogen and vacancies act to reduce the lattice parameter of pure NbC. Figure 1 further illustrates that the extent to which the lattice parameter is lowered with increased nitrogen will depend on the vacancy concentration of the carbonitride. The higher the vacancy concentration, the larger will be the lowering of lattice parameter per unit increase in nitrogen content in the carbonitride. Storms and Krikorian [18] point out that the interpretation of lattice parameter measurements will be difficult unless the vacancy concentration in the carbonitride can be assessed.

Composition of NbC_xN_y Formed in Niobium Steels

The composition of precipitates found in commercial steels has been extensively studied and the results obtained prior to 1973 were reviewed by Gray [19]. Briefly, it can be stated that the cubic forms of carbonitride are most frequently found at normal niobium levels (<0.04%). The reported range of stability from $\text{NbC}_{0.72}$ to $\text{NbC}_{1.0}$ [20,21] may allow substitution of molybdenum [22,23] as well as the

nitrogen/vacancy contents discussed earlier without causing changes in crystal structure.

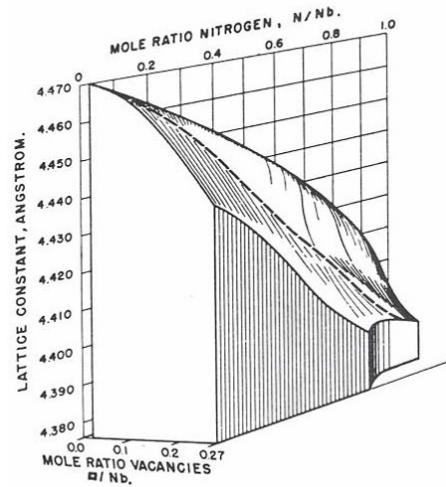


Figure 1. Lattice parameter versus composition in the NbN-NbC system [16-18].

Other studies of the composition of the carbonitride which forms in Nb-bearing microalloyed steels [10-13, 24-26] have shown a direct relationship between the composition of the carbonitride and the composition of the steel; the larger the N/C ratio in the steel, the more nitrogen-rich the carbonitride. A typical example of the relation is shown in Figure 2 [12].

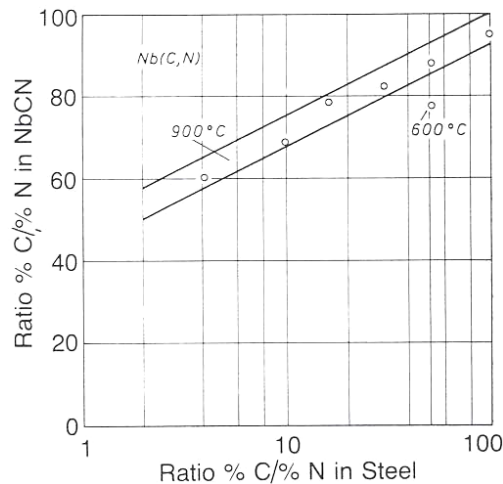


Figure 2. Influence of C/N ratio in 0.1 percent Nb steel on C/N ratio in carbonitride precipitate [12].

These and other studies [19,27-30] have also shown that the composition of the carbonitrides in any given steel can depend upon the thermal conditions under which they form. The data indicate that the precipitates contain more nitrogen when formed at higher temperatures [11, 13, 30, 31], depending on C content, Figures 3 and 4 [30], which is similar to results for precipitation of vanadium carbonitride in vanadium-strengthened microalloyed steels [31,32].

It is to be expected that the presence of other elements such as titanium and aluminum, that have strong nitride-forming tendencies, will affect the amount of nitrogen in NbC_xN_y . This has been observed by Ouchi, et al. [26] especially in steels austenitized at high temperatures, Figure 5.

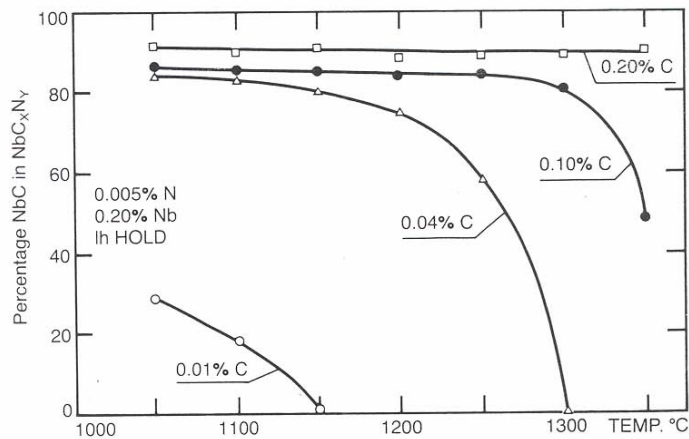


Figure 3. Change in NbC_xN_y composition as a function of carbon content and precipitation temperature [30].

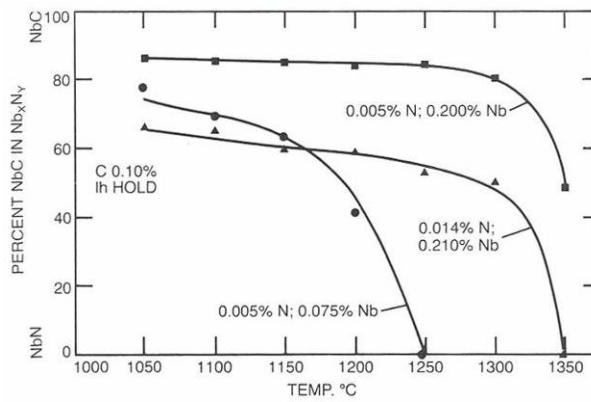


Figure 4. Change in NbC_xN_y composition with Nb content and precipitation temperature [30].

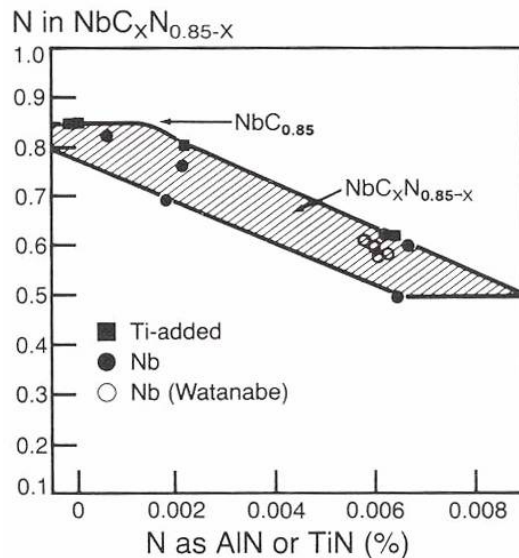


Figure 5. The relationship between the nitrogen content uncombined with Al or Ti and the composition of niobium carbonitride [26].

Long austenitizing treatments (≥ 150 h) and higher niobium ($\geq 0.10\%$) and nitrogen contents ($\geq 0.012\%$) give rise to the formation of non-cubic compounds, often of the hexagonal NbC- δ' or NbC- ε carbonitride type [27-29]. Also, as stated earlier, Nb₂C-(NbC- β) type precipitates are observed at high Nb/C mole ratios [19,33].

The Solubility of NbC_xN_y in Austenite

The formation (and dissolution) of precipitates normally exhibits sigmoidal kinetic curves which can be approximated by the Kolomojorov-Johnson-Mehl-Avrami (KJMA) equation [34].

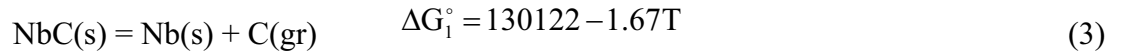
$$X_p = 1 - \exp\left(-\frac{\pi}{3} N \dot{G}^3 t^4\right) \quad (1)$$

where: X_p = fraction of precipitates formed
 N = nucleation rate (usually assumed constant)
 \dot{G} = growth rate (usually assumed constant)
 t = reaction time.

The equation shows that a precipitation reaction will attain a given level of completion only when N , \dot{G} and t have sufficiently large values. The nucleation rate is controlled by solute supersaturation while the growth rate is controlled by both the diffusion coefficient and the solute supersaturation [35]. Since solute supersaturation controls both N and \dot{G} , it is very important to understand the factors that determine it. The extent to which elements can be maintained in solid solution in austenite is governed by the appropriate solubility product. If, for example, we are interested in the extent of solid solubility of Nb and C in austenite which is in equilibrium with pure, stoichiometric NbC, then we must consider this reaction [36].



And at equilibrium, the reaction can be written as follows:



where ΔG_1° represents the positive change in free energy (joules/mole) for the above reaction. It is important to realize that in this reaction, NbC, Nb(s) and C(gr) are taken as the pure components in a stable state of existence at some given temperature. This is referred to as the Raoultian standard state [37,38]. For cases where the pure component may exist in a physical state which is different from that of the solution, the Henrian 1 weight percent standard state may be more convenient.

The Henrian standard state is obtained from Henry's law, which, strictly being a limiting law obeyed by the solute Nb (or C) at infinite dilution in austenite, is expressed as: [38]

$$\frac{a_{\text{Nb}}}{X_{\text{Nb}}} \rightarrow \gamma_{\text{Nb}}^\circ \quad \text{as} \quad X_{\text{Nb}} \rightarrow 0 \quad (4)$$

where a_{Nb} is the activity of Nb in austenite with respect to the Raoultian standard state, X_{Nb} is the mole fraction of Nb in solution and γ_{Nb}° is Henry's law constant. Henry's law constant is the activity coefficient which quantifies the difference between Raoultian solution behavior of Nb and Henrian solution behavior of Nb [38]. If the solute (Nb or C) obeys Henry's law over a finite composition range, then:

$$a_{\text{Nb}} = \gamma_{\text{Nb}}^\circ X_{\text{Nb}} \quad (5)$$

The Henrian standard state is obtained by extrapolating the Henry's law line deviating from ideal solution behavior to $X_{\text{Nb}} = 1$. This state represents pure Nb in the hypothetical, non-physical state in which it would exist as a pure component if it obeyed Henry's law over the entire composition range (i.e., as it does for a dilute solution) [37,38].

Having defined the Henrian standard state, the activity of Nb in solution in austenite (h_{Nb}) with respect to the Henrian standard state having unit activity is given by:

$$h_{\text{Nb}} = f_{\text{Nb}} X_{\text{Nb}} \quad (6)$$

where f_{Nb} is the Henrian activity coefficient.

It should be noted that the mole fraction of Nb in solution in austenite can be related to its concentration in weight percent by:

$$X_{\text{Nb}} = \frac{\frac{\text{wt}\% \text{Nb}}{\text{MW}_{\text{Nb}}}}{\frac{\text{wt}\% \text{Nb}}{\text{MW}_{\text{Nb}}} + \frac{(100 - \text{wt}\% \text{Nb})}{\text{MW}_{\text{Fe}}}} \quad (7)$$

where MW_{Nb} and MW_{Fe} are the respective atomic weights of Nb and Fe. This conversion is necessary in order that a hybrid Henrian standard state can be introduced. This is referred to as the 1 wt% standard state. This standard state differs from the previous one in that a weight percent coordinate system is used rather than a mole fraction coordinate system. The use of this standard state eliminates the necessity of converting weight percentages, obtained via chemical analysis, to mole fractions for the purpose of thermodynamic calculations. This standard state is particularly convenient to use in metallurgical systems containing dilute solutes [37,38]. This standard state can formally be defined as:

$$f_{\text{Nb}} \rightarrow 1_{\text{as}} \quad \text{wt}\% \text{Nb} \rightarrow 0 \quad (8)$$

Hence, with respect to the 1 wt% standard state having unit activity, the activity of Nb is given by:

$$h_{\text{Nb}} = f_{\text{Nb}} \cdot \text{wt}\% \text{Nb} \quad (9)$$

This expression for the activity of Nb is often simplified by two further assumptions which reduce f_{Nb} to unity. These assumptions are often made in the calculation of the equilibrium constant (K), also referred to as the solubility product [24]. The first of these assumes that Nb is a dilute solute in austenite. The second assumption neglects any interaction between solutes in the system. The fact that f_{Nb} goes to unity under these assumptions can be realized given the dependence of f_{Nb} on the first order free energy interaction coefficient for dilute, multi-component solutions [39,40]. This interaction coefficient was first introduced by Wagner [39] and later was extensively used by Chipman [40] and colleagues in the study of molten alloy steels. It is related to the activity coefficient such that:

$$\log f_i = \sum_{j=1}^n e_i^j (\text{wt}\% j) \quad (10)$$

where e_i^j , (read "e j on i") is the Wagner interaction parameter on a weight percent composition coordinate and n would represent the total number of solute elements or compounds in the system [39]. It is apparent from Equation 14 that if either a solute is dilute in a given system ($\text{wt}\% j \rightarrow 0$) or that

interactions between solutes are negligible ($e_i^j \rightarrow 0$), the activity coefficient for the given solute will be unity.

Returning to the dissolution of NbC precipitates, the change in free energy (joules/mole) as C and Nb are dissolved in austenite is given by: [24]

$$C(\text{gr}) = [C] \quad (11)$$

$$Nb(\text{s}) = [Nb] \quad \Delta G_3^\circ = -27949 - 29.54T \quad (12)$$

where ΔG_2° and ΔG_3° represent the free energies associated with the change between the Raoultian and Henrian standard states. The overall reaction is given as:

$$NbC = [Nb] + [C] \quad (13)$$

The corresponding change in free energy is given by the addition of Equations 7,15, and 16:

$$\Delta G^\circ = 137235 - 64.43T = -2.303 \cdot R \cdot T \cdot \log \frac{h_{Nb} h_C}{a_{NbC}} \quad (14)$$

where a_{NbC} is taken as unity for the pure component NbC in its standard state. Furthermore, assuming that Nb and C are dilute in austenite, h_{Nb} and h_C may be represented by their weight percents. Hence, the solubility product under this theoretical treatment is found to be:

$$\log[Nb] \cdot [C] = 3.36 - \frac{7167}{T} \quad (15)$$

There are three things that must be taken into account when applying a solubility product of the form shown above that has been derived from thermodynamic considerations:

- i) It applies strictly to equilibrium conditions that rarely exist in practice,
- ii) It might be strongly altered by the presence of other solutes through their effect on the interaction coefficients presented above, and
- iii) It will surely be altered by the Gibbs-Thompson or capillarity effect that accounts for the influence of particle curvature on solubility. The solubility of a given particle varies inversely with its curvature [41,42]. Following Lupis, the solubility of particles of radius 1nm would be nearly twice as high as those of radius 100 nm [42].

Nb(CN) Solubility Products in Austenite

The importance of Nb as a microalloying element in steels is apparent from the numerous studies over the past 30 years. Much of this work is concerned with the solubility of niobium monocarbides [7,24,43-50], mononitrides [7,24,49-51] and carbonitrides [2,7,13,51-54] in austenite. The results of these studies are shown in Table I in the form of solubility products. The differences among these products are considerable and may be attributed to a number of reasons. Foremost among these reasons would be the methods used in obtaining the given solubility product as each technique has its own assumptions and limitations. These techniques used in obtaining the solubility products of Table I are

classified as a-e and are briefly described below:

- a) Thermodynamic calculations
- b) Chemical separation and isolation of precipitate
- c) Equilibrating a series of steels with different Nb contents with a H₂-CH₄ atmosphere at various temperatures, after which the carbon contents are analyzed
- d) Hardness measurements
- e) Statistical treatment of previous solubility products.

As was stated in the previous section, thermodynamic calculations of solubility products often neglect any interaction between elements and particle curvature effects. As a result, the activity coefficients are assumed to be unity and the activities are represented by their weight percents [20]. Later work, however, by Koyama et al. [55] and Sharma et al. [47] has included Wagner interaction parameters to account for the effect of alloying elements on the solubility of Nb(CN) in austenite. This leads to a more realistic solubility product since it incorporates non-unity activity coefficients.

Table I. Solubility products for Nb-C, Nb-N and Nb-C-N systems in austenite

System	Product	Method	Reference
Nb-C	$\text{Log[Nb][C]} = 2.9 - 7500/T$	d	24
	$\text{Log[Nb][C]} = 3.04 - 7290/T$	b	24
	$\text{Log[Nb][C]} = 3.7 - 9100/T$	c	43
	$\text{Log[Nb][C]} = 3.42 - 7900/T$	b	50
	$\text{Log[Nb][C]} = 4.37 - 9290/T$	c	44
	$\text{Log[Nb][C]}^{0.87} = 3.18 - 7700/T$	b	45
	$\text{Log[Nb][C]}^{0.87} = 3.11 - 7520/T$	e	24
	$\text{Log[Nb][C]} = 2.96 - 7510/T$	e	24
	$\text{Log[Nb][C]}^{0.87} = 3.4 - 7200/T$	a	24
	$\text{Log[Nb][C]} = 3.31 - 7970/T + \phi$	b	46
	$\text{Log[Nb][C]}^{0.87} = 2.81 - 7019.5/T$	a	47
	$\text{Log[Nb][C]} = 1.18 - 4880/T$		49
	$\text{Log[Nb][C]} = 3.89 - 8030/T$		49
	$\text{Log[Nb][C]} = 4.04 - 10230/T$	c	51
	$\text{Log[Nb][C]} = 3.79 - 10150/T$	b	45
Nb-N	$\text{Log[Nb][N]} = 2.8 - 8500/T$	b	50
	$\text{Log[Nb][N]} = 3.7 - 10800/T$	b	53
	$\text{Log[Nb][N]}^{0.87} = 2.86 - 7927/T$	a	47
	$\text{Log[Nb][N]} = 4.2 - 10000/T$		49
Nb-C-N	$\text{Log[Nb][C]}^{0.24}[\text{N}]^{0.65} = 4.09 - 10500/T$	b	24
	$\text{Log[Nb][C + 12/14N]} = 3.97 - 8800/T$	c	13
	$\text{Log[Nb][C + N]} = 1.54 - 5860/T$	b	24
	$\text{Log[Nb][C]}^{0.83}[\text{N}]^{0.14} = 4.46 - 9800/T$	b	24
	$\text{Log[Nb][C + 12/14N]} = 2.26 - 6770/T$	c	52

Note $\phi = [\text{Mn}](1371/T - 0.9) - [\text{Mn}]^2(75/T - 0.0504)$

Although techniques such as chemical separation and methane equilibration indirectly account for chemical interactions, both have their own limitations. Problems arising from the separation technique are that very fine precipitates may not be included in the analysis [48] and that discrepancies may exist

as to the exact composition of the precipitate. [24] These problems also plague the equilibration methods, as carbon contents are often analyzed assuming that a uniform stoichiometric or non-stoichiometric compound is present [24,48]. Additionally, both of these methods, including the thermodynamic methods, neglect the effect of precipitate size on solubility. Thermodynamics indicate that small particles are more soluble than large particles [56]. Hence, solubility products obtained via these methods may predict a more stable precipitate than would be expected. A possible exception to this may be found in the work by Simoneau et al. [57] who used electrical resistivity measurements to determine the solubility of Nb(CN) in austenite. This technique is based upon the measured reduction in bulk resistivity as Nb, C and N in solid solution precipitate to form Nb(CN). The reduction in resistivity is caused by the loss of solid solution atoms which act as scattering centers. The results of Simoneau et al. [57] show that the thermodynamic stability of Nb(CN) is less than that predicted using equilibrium methods.

Finally, hardness techniques are questionable since they are based upon the assumption that an increase in hardness is proportional to the amount of Nb dissolved into austenite, and subsequently precipitated in ferrite as NbC [24]. Although this does occur, all of the carbon and nitrogen in the alloy is not necessarily associated with the precipitate. Also, difficulties arise in separating this hardness increment from those due to other mechanisms such as grain size strengthening, solid solution strengthening and dislocation strengthening.

A comparison between some of the solubility relations listed in Table I is shown in Figure 6 [7]. This diagram depicts the solubility product in austenite, K , versus temperature. The results shown by Figure 6 indicate two important points. First, the solubility product is substantially lowered as the compound becomes enriched in nitrogen. Second, the solubility of a precipitating compound in austenite is decreased as the vacancy content becomes smaller. Solubility products play a vital role in understanding the physical metallurgy of microalloyed steel, especially those aspects which are concerned with precipitation-related phenomena. Solubility products can be plotted in either of two ways. Consider the case of the solubility product of NbC in austenite at some given temperature. If the abscissa (C) and ordinate (Nb) axes have a linear scale, then any given solubility isotherm will have the shape of a hyperbola. If, however, the axes have a logarithmic scale, then the solubility isotherm will be a straight line. Both approaches have been widely used in the literature.

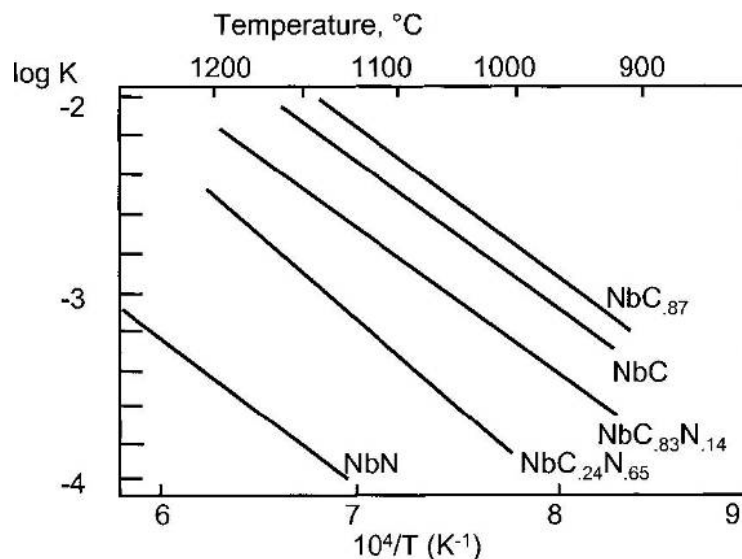


Figure 6. Solubility products for various Nb precipitates in austenite [7,24].

A hypothetical solubility isotherm for NbC in equilibrium with austenite at 1000°C is shown in Figure 7(a) [7]. The solubility isotherm gives the locus of Nb and C products which represents the limit of solid solubility of NbC in austenite at 1000°C, i.e. any combination of products located above the line will be in the $\gamma + \text{NbC}$ phase field at 1000°C. The straight line with a positive slope on the diagram represents the stoichiometric ratio. The precipitation of NbC can be followed by considering the slightly curved line which is nearly equidistant from the stoichiometric line and passes through the point with the Nb and C coordinates which describe the composition of the steel. A schematic illustration is presented in Figure 7(b). Consider a steel of composition given by point B which is reheated to 1300°C and is very slowly cooled to 900°C. Since 1300°C is the solution temperature for the NbC under consideration here, the NbC can be assumed to be completely dissolved after reheating. If we further assume that precipitation occurs during the cooling, then the composition of the austenite in equilibrium with NbC would move along the curve passing through point B and which is equidistant from the stoichiometric line. The distance moved along the curved line through point B is proportional to the volume fraction of precipitate formed as a result of the cooling, assuming equilibrium is established at all temperatures. In other words, the distance moved along the curved line through B during cooling is proportional to the supersaturation and would also be proportional to the volume fraction precipitate formed if equilibrium prevailed. Therefore, if steel B is reheated to 1300°C and then cooled to and rolled at 900°C, the distance BC in Figure 7(b) will be proportional to the volume fraction of precipitation of NbC formed in austenite. This precipitation would be of two types: that formed during cooling and that formed during or after rolling. The first type is not likely to be significant since precipitation in recrystallized austenite is normally very sluggish, as will be discussed later. The second type is the strain-induced precipitation. A second interesting case would occur if steel of composition A in Figure 7(b) is considered. If this steel is reheated at 1300°C and hot rolled at 900°C, then two arrays of NbC particles would be expected. The first would be the precipitates that survived the reheating treatment (volume fraction proportional to AB) and the second strain-induced precipitate (volume fraction proportional to BC).

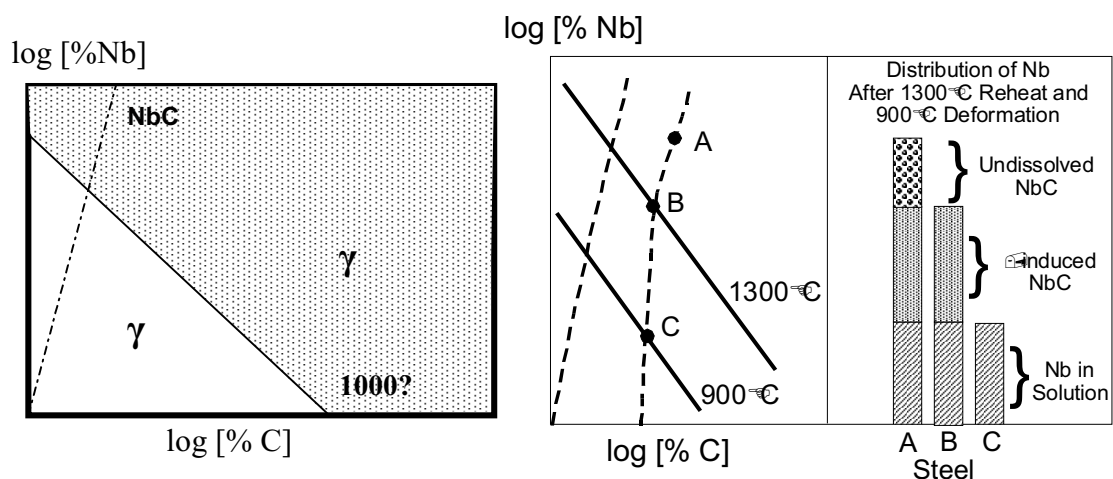


Figure 7. Hypothetical solubility diagrams describing equilibrium between NbC and austenite: (a) relationship at 1000 C and (b) interrelationships among isotherms, steel composition, processing and potential amount of precipitation [7].

Several investigators have used solubility diagrams to help explain the physical metallurgy of microalloyed steels, and, in particular, the precipitation phenomena [57-59]. Our understanding of precipitation in these steels has been substantially increased by the work of Wadsworth et al., [60] Roberts et al., [31] and Keown and Wilson [61]. The study by Wadsworth et al. [60] concluded that the supersaturation that could be developed between any two temperatures is a strong function of the position of the steel relative to precipitate stoichiometry on the solubility diagram. This effect,

illustrated in Figure 8, shows that the largest possible supersaturation occurs when the microalloying element and the interstitial are present in the steel in the stoichiometric ratio, and deviations from this ratio will lead to decreasing supersaturations.

The work of Roberts et al. [31] presents an interesting way of considering the precipitation of carbonitride precipitates in microalloyed steels. They suggest a thermodynamic analysis which attempts to predict the change of x and y in VC_xN_y with changes of temperature and/or extent of precipitation. Their model predicts that nitrogen-rich precipitates are the first to form and that nitrogen plays a central role in controlling the precipitation until it is completely consumed.

As stated above, solubility products can be influenced by the presence of elements that do not directly participate in the precipitation reaction. This effect occurs through the influence of third and higher order elements in solution on the interaction coefficients, hence activities, for Nb and C in austenite. Third elemental solutes that raise the activity of Nb or C through a positive interaction coefficient decrease their solubility while those that decrease the activity through negative coefficients increase it. Interaction coefficients for C, N, and Nb in liquid steel at 1600°C are shown in Table II [62]. Unfortunately, similar data for these species in austenite at 1000°C, for example, do not exist at this time. If we assumed that the data of Table II did apply to austenite at 1000°C, then we would find that certain solutes would increase the solubility of C and Nb in austenite, leading to less than expected NbC, while others would decrease it, leading to more.

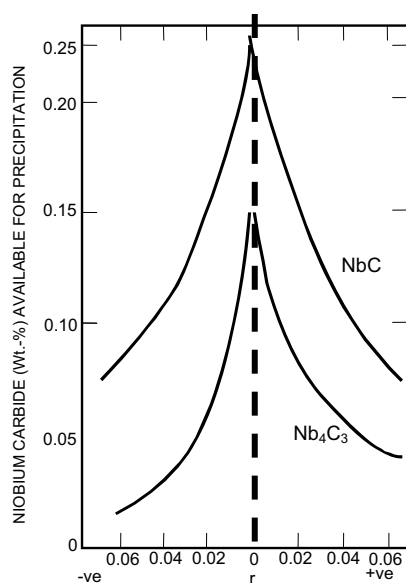


Figure 8. Amount of niobium carbide available for precipitation at 923 K (after solution-treatment at 1373 K) as function of degree of deviation from stoichiometry, r . Positive values of r indicate C-rich compositions, negative values Nb-rich [60].

Examples of this effect have been studied by Koyama, et al. [55] who have examined the influence of several elements on the solubility of NbC in austenite. By way of an example, the solubility product for NbC in otherwise unalloyed austenite is about 5×10^{-3} at 1150°C. An addition of Mn increased $\log K$ by about 5% per % Mn added, while an addition of Si reduced $\log K$ by about 45% per % Si added. The solubility product at 1150°C for a steel that contained 1.5% Mn and 0.4% Si was $\cong 4 \times 10^{-3}$; the addition of Mn and Si acted to reduce the solubility product by about 20%.

The latest and perhaps the most accurate solubility product for nominally stoichiometric NbC in austenite in a steel containing 0.08C-1.5Mn-0.008N-0.02Nb was published by Palmiere et al. in 1994 [63]. The following expression was derived from solubility data obtained from reheated and quenched samples as measured using the atom probe facility of an atom probe field ion microscope (APFIM):

$$\text{Log [Nb][C]} = 2.06 - 6700/T \quad (16)$$

It is important to note that a comparison of this product with several earlier ones indicates that the earlier products substantially overestimated the amount of Nb in solution in austenite and underestimated the dissolution temperature [63]. This product has been used successfully in subsequent research [64].

Table II. Influence of several selected elements on the interaction coefficients for C, N, and Nb in liquid iron at 1600°C [62]

Solute	C	N	Nb
Al	5.3	5.2	
C	6.9	5.86	-23.7
Cr	-5.1	-10	
H	3.8		-1.5
Mn	-2.7	-8.1	
Mo	-4	-4.9	
N	5.86	0.8	
Nb	-23.7	-26	-26
Ni	2.9	1.5	
O	-22	4.0	-54
P	7	6.2	
S	6.5	1.4	-5.8
Si	9.7	5.9	

Solubility of NbCN in Ferrite

It is well known that the solubility of various elements is higher in austenite than in ferrite [65,66]. An example, published in 1994, for the solubility of various microalloyed carbides and nitrides in austenite and ferrite in an ultra-low carbon steel is shown in Figure 9 [67,68]. At about the same time, solubility products for various microalloyed precipitates in ferrite were published by Taylor [69].

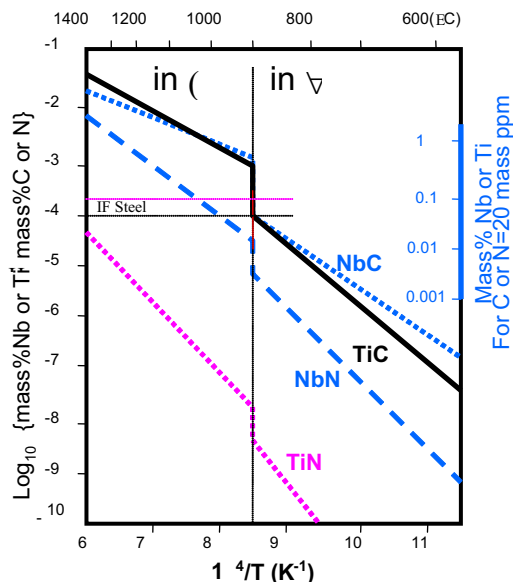


Figure 9. Solubility for each pure compound, NbC, TiC and TiN in austenite and ferrite [67,68].

It is interesting to compare the expected behavior for MC in austenite and ferrite for the various microalloying elements. One way that this can be accomplished is by comparing the solubility limits for the various carbides in austenite and ferrite at a given temperature, for example, near a typical Ar3. The result of using this approach is shown in Table III below, where the solubility limits in austenite and ferrite were calculated at 800°C using the products suggested by Taylor [69]. This table shows that the limiting product for NbC is reduced by a factor of near 20 when going from austenite to ferrite at 800°C.

A more encompassing discussion of solubility products, covering a wide variety of precipitates, can be found in the recent work of Gladman [70].

Although the use of solubility products is helpful in understanding the behavior of microalloying elements in austenite and ferrite, there are some important restrictions that must be recognized when applying them. The question is one more of validity than accuracy. It is indeed true that precipitation reactions are controlled by solubility relations; however, the major question is what should be considered the proper matrix composition. In most cases, the bulk composition is used to calculate, for example, the dissolution temperature of a precipitate in austenite. However, many precipitate reactions are governed by a local composition rather than a bulk composition. Hence, the influence of segregation on precipitation must be considered when applying any solubility equation. This point has been discussed in some detail by Palmiere et al. [64]

Table III. Comparative Solubility Limits for MC in Austenite and Ferrite at 800°C

Solubility Product	$[M][C] \times 10^4$
NbC in γ	8.9×10^{-5}
NbC in α	4.5×10^{-6}
TiC in γ	1.7×10^{-4}
TiC in α	3.0×10^{-5}
VC in γ	7.9×10^{-3}
VC in α	1.1×10^{-3}

Crystallography of Precipitation: Orientation Relationships and Lattice Matching

The crystallography of precipitation in steel has been reviewed by Jack et al. [71], Davenport et al. [72], and Honeycombe [73]. There are two aspects of the crystallography of precipitation that are of interest in this discussion. These are (a) the orientation relationship that exists between the crystal structure of the precipitate and that of the matrix, and (b) the degree of lattice registry between the precipitate and the matrix.

Carbonitrides of niobium, vanadium and titanium can precipitate in both austenite and ferrite. Several studies [74-77] have shown that when these carbonitrides precipitate in austenitic stainless steel, they do so such that the lattice of the precipitate, which has a NaCl crystal structure, is parallel to the FCC lattice of the parent austenite, i.e.

$$\begin{aligned} [100]_{M(CN)} &\parallel [100]_{\gamma} \\ [010]_{M(CN)} &\parallel [010]_{\gamma} \end{aligned}$$

Davenport et al., have provided direct evidence that this same relationship holds for the strain-induced precipitation of NbC in austenite in a microalloyed steel [72]. When NbC_xN_y precipitates in ferrite [72,73] or martensite [78], it does so with the Baker-Nutting orientation relationship [78].

$$\begin{aligned} [100]_{NbC} &\parallel [100]_{\alpha} \\ [011]_{NbC} &\parallel [010]_{\alpha} \end{aligned}$$

The “parallel” and Baker-Nutting orientation relationships can be simply illustrated through the use of the appropriate metal-atom octahedral [71]. The metal-atom octahedra for austenite, NbC_xN_y and ferrite are shown in Figure 10 [71]. The structures of the austenite and NbC_xN_y are positioned to represent the parallel orientation relationship and the structures of the ferrite and NbC_xN_y are positioned to represent the Baker-Nutting orientation relationship. Note that the three octahedra shown in Figure 10 all have a cube plane at the base.

The octahedra shown in Figure 10 also permit the calculation of lattice misfit strain or the lattice strain required for coherency. This is done by calculating the linear strain in the matrix lattice parameter that would be required to bring the two lattices into coincidence at the matrix-precipitate interface, i.e.

$$\% \text{Linear Strain} = \frac{L_p - L_m}{L_m} \times 100 \quad (17)$$

where L_p = appropriate length of octahedron of the precipitate, and
 L_m = appropriate length of octahedron of the matrix.

Examples of the required strain or strain of the matrix for several types of precipitates are shown in Table IV. The magnitudes of the elastic matrix strains ($\epsilon = 0.255$ for NbC in austenite and $\epsilon = 0.105$ and 0.563 in ferrite) required for lattice registry would appear to rule out any large degree of coherency between the precipitate and the matrix. However, the elastic strains required of the matrix to achieve partial lattice registry could be easily accommodated by the presence of a few interfacial dislocations for a precipitate of dimension 100 \AA .

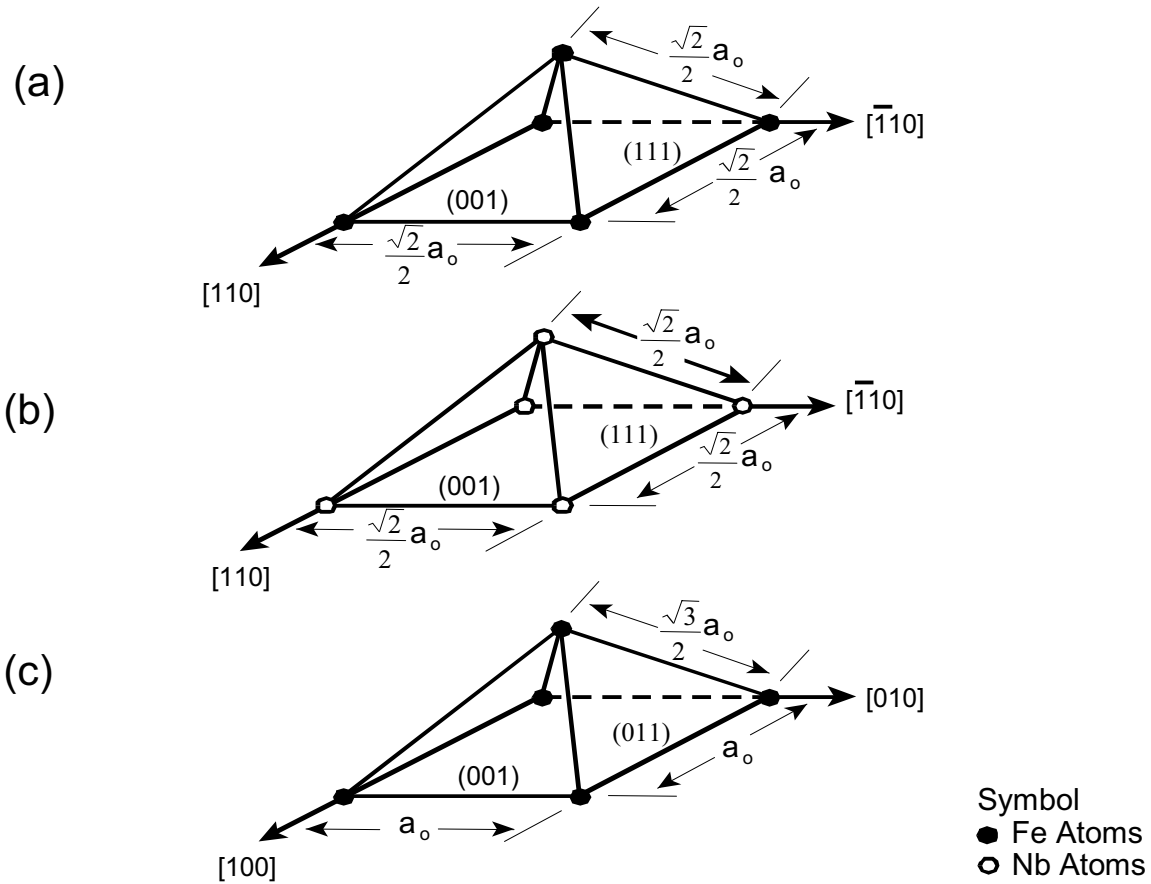


Figure 10. Metal-atom octahedra for (a) austenite, (b) NbC and (c) ferrite [71].

Table IV. Lattice Mismatch for NbC_xN_y Precipitates in Austenite and Ferrite

Matrix	Orientation Relationship	Required Linear Strain in Matrix, % ^ψ		
		NbC	NbC ₈	NbN ₈
γ	$[100]_{\text{ppt}} \parallel [100]_{\gamma}$	25.5	26.6	23.0
	$[010]_{\text{ppt}} \parallel [101]_{\gamma}$	25.5	26.6	23.0
	$[001]_{\text{ppt}} \parallel [001]_{\gamma}$	25.5	26.6	23.0
α	$[100]_{\text{ppt}} \parallel [100]_{\alpha}$	56.3	57.7	53.1
	$[011]_{\text{ppt}} \parallel [010]_{\alpha}$	10.5	11.5	8.4
	$[011]_{\text{ppt}} \parallel [001]_{\alpha}$	10.5	11.5	8.4

^ψ All matrix strains are tensile (+).

A first-order approximation indicates that about seven and three dislocations would be required to cancel the lattice mismatch for a precipitate of NbC of size 100 Å in austenite and ferrite, respectively.

The orientation relationship that is observed between the NbC and ferrite can be used to distinguish the NbC which had nucleated in austenite from the NbC which had nucleated in ferrite. As was noted above, NbC forms in austenite with a parallel orientation relationship and in ferrite with the Baker-Nutting orientation relationship. Therefore, all NbC precipitates that show the Baker-Nutting relationship must have formed in the ferrite. The NbC that forms in austenite will not have the Baker-Nutting relationship with the ferrite.

When austenite transforms to ferrite or martensite, it does so with the Kurdjumov-Sachs orientation relationship [80].

$$\begin{array}{l} (111)_\gamma \parallel (110)_\alpha \\ [110]_\gamma \parallel [111]_\alpha \end{array}$$

The consequence of this relationship is that when the matrix transforms from austenite to ferrite, the orientation of the original austenite and the precipitates that formed in that austenite would be related to the ferrite by the Kurdjumov-Sachs relationship. Therefore, the precipitates that formed in the austenite can be identified because they will have the Kurdjumov-Sachs orientation relationship with the ferrite when observed at room temperature. If the orientation of the austenite grains would change after precipitation had occurred, e.g. by grain rotations accompanying deformation or recrystallization, then there would be no rational crystallographic relationship between the NbC that had formed in the austenite and the final ferrite matrix. In principle, this change in austenite grain orientations after precipitation would not appear to be a very frequent occurrence since most of the precipitation that forms in austenite is strain-induced, and these precipitates act to suppress subsequent recrystallization of the deformed austenite in which they formed. [Hereinafter, NbCN will be used to denote NbC_xN_y].

Precipitation of NbCN: Typical Morphologies and Distributions

The precipitation of NbCN in austenite and ferrite is heterogeneous in nature, i.e. it always occurs in conjunction with crystalline defects such as grain boundaries, incoherent twin boundaries, stacking fault boundaries, subgrain boundaries, or dislocations. One reason why the precipitation forms in this fashion is the rather large mismatch between the lattice of NbCN and the matrix, austenite [16,19-21,33,50], or ferrite [13,20,22-28,33,81], as shown in Table IV. These crystalline defects are sources of dislocations which can act to cancel some of the elastic strain which may develop during the formation of the precipitates.

In one of the few studies that have been conducted on the precipitation of NbCN in recrystallized austenite, Santella has shown that the NbCN forms almost exclusively on grain boundaries [13] as is the case for precipitation in casting [28]. Much more research has been done on NbCN precipitation which has formed in deformed austenite and in ferrite. Good illustrations of strain-induced precipitates of NbCN in deformed austenite are available in the literature [82-87], and an example is presented in Figure 11 [13]. In every case, the precipitates appear to decorate what was once a grain or subgrain boundary in the prior-austenite.

When NbCN precipitates in ferrite, the nature of the precipitate distribution is related to the nature of the austenite-to-ferrite transformation. If the ferrite that forms has a polygonal morphology, the NbCN precipitation will have the “interphase” distribution [72,73]. During the interphase precipitation, the NbCN forms along the advancing austenite-ferrite phase boundary. When the boundary moves to a new location, the precipitates are left behind in a sheet-like array. The final microstructure consists of numerous sheets of precipitates, where each sheet denotes the location of the interphase boundary during the course of the transformation. This form of precipitation in Nb steels has been observed by Gray and Yeo [88] and others [72,89,90], and an example is given in Figure 12 [13]. It should be noted that this form of precipitation only occurs at very high temperatures in ferrite. When precipitation occurs substantially after transformation is complete, the precipitate has a more uniform or general distribution [88]. These precipitates are responsible for the precipitation hardening effect of NbCN.

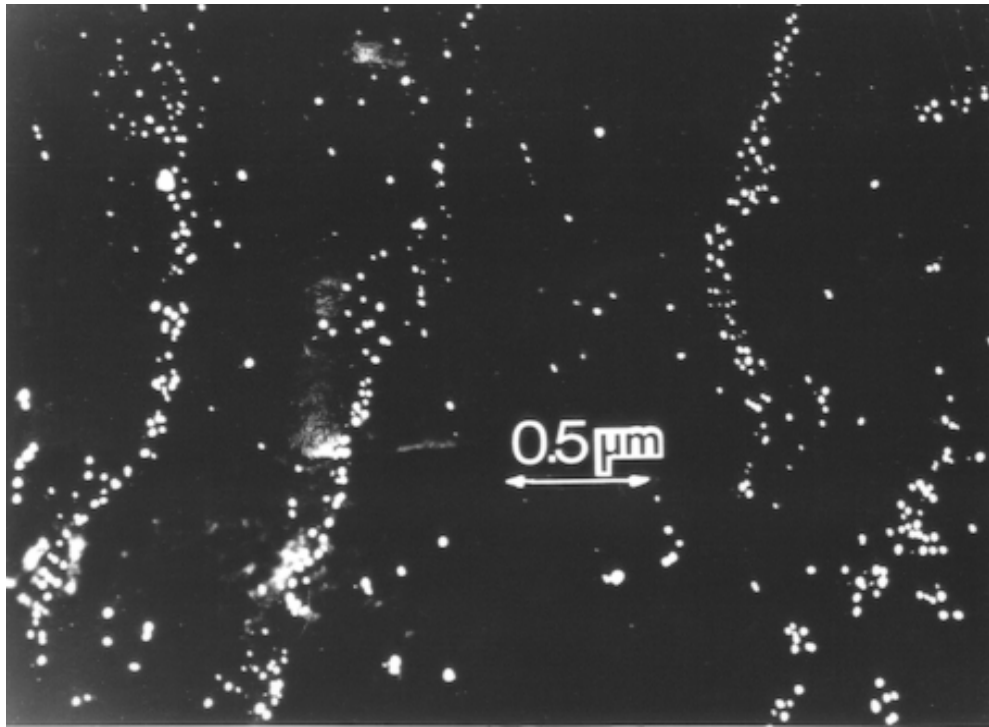


Figure 11. Strain induced precipitation of NbCN in austenite in a steel containing 0.09%C - 0.07%Nb. Specimen reheated at 1250°C, rolled 25% and held at 950°C, and air cooled to RT. Centered dark field electron micrograph using a (111) NbC reflection [13].

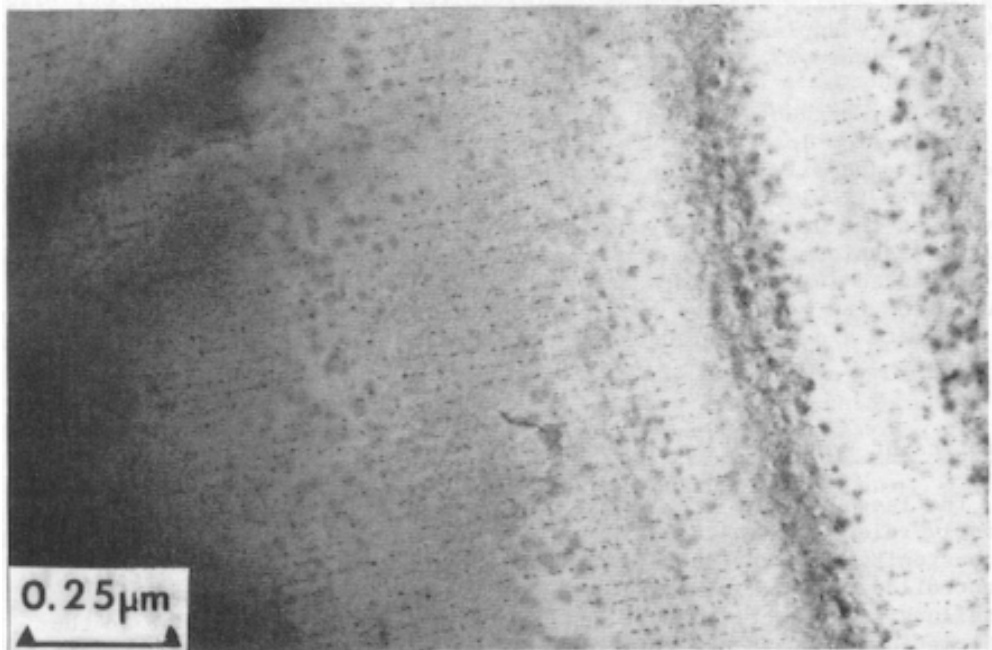


Figure 12. Interphase precipitation of NbCN in ferrite in steel containing 0.09%C - 0.07%Nb. Specimen was reheated to 1250°C, hot rolled to 1000°C and air cooled to RT. Bright field electron micrograph [13].

Similar general distributions occur in ferrite which has an acicular or bainitic character [72]. Furthermore, there is great similarity in distributions and morphologies between the NbCN that forms in acicular ferrite and the NbCN that forms during secondary hardening in the tempering of a quenched

steel [78]. An example of this general type of precipitation of NbCN in acicular ferrite is given in Figure 13 [13].

Thermomechanical Processing and Austenite Conditioning in Nb Steel

Background

Although Nb can play many important roles in steel, none is more important than austenite conditioning. Here, austenite conditioning means having the terminal hot rolled austenite with the proper microstructure and composition to allow the desired final ferrite microstructure to be achieved after suitable cooling. For simple ferrite-pearlite steels, this means controlling (increasing) the crystalline defect content of the austenite that can act as nucleation sites for ferrite upon transformation. This was the original view of austenite conditioning and was widely discussed in the early 1980's. These defects, as we shall see, include grain boundary area, deformation band area, and incoherent twin boundary area per unit volume. This catalytic effect has been discussed earlier [91-93]. In the past 20 years, we have expanded this view of austenite conditioning and its benefits to include acicular ferrites, bainites and martensites [94]. Furthermore, the benefits of austenite conditioning have been extended to high strength strip and sheet with improved stretch forming, e.g., the dual-phase and TRIP steels. Here, the distribution of low temperature transformation products their contribution to work hardening is controlled by the defect structure of the austenite [95-102]. This work shows that the finer the austenite, the finer the distribution of low temperature transformation products, the higher the work hardening rate and the resulting stretch formability.

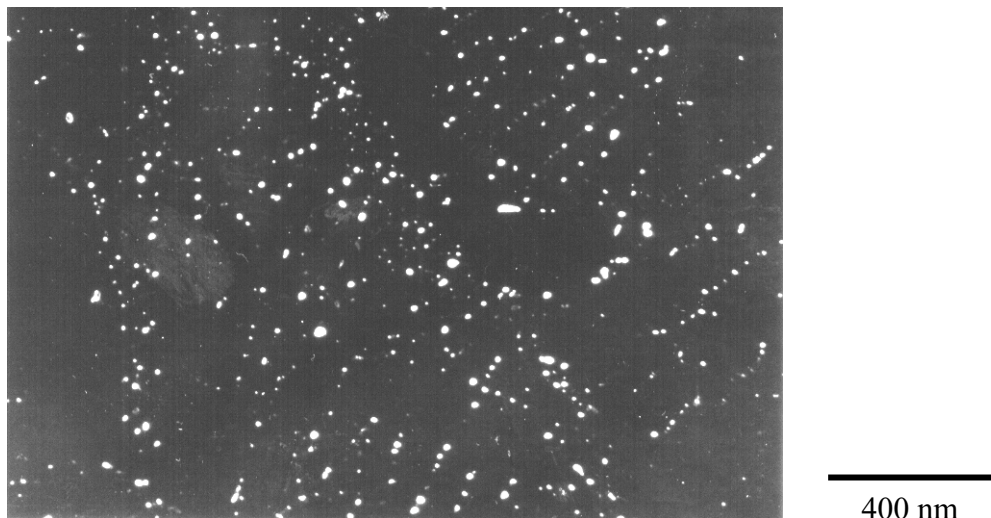


Figure 13. General precipitation of NbCN in austenite in a steel containing 0.09%C - 0.07%Nb. Specimen reheated at 1250°C, hot rolled to 1000°C and air cooled to RT. Centered dark field electron micrograph using a (111) NbC reflection [13].

Role of Processing

Before the role of Nb in austenite conditioning can be discussed, it is important to briefly review the various commercial rolling practices being used. Since Nb can act as either a solute or precipitate in austenite, each with different effects, it is important to recognize where the Nb would be during rolling, and this will vary with the rolling practice. For precipitation to occur in austenite, there must exist adequate levels of both supersaturation and interpass time. Hence, slow processing in austenite, typical

of reversing plate and heavy section rolling, where the rolling involves many light passes with long interpass times and long total rolling times, is rather ideal for extensive static precipitation of NbCN in austenite. However, fast processing of austenite, such as found with strip or bar rolling, where both the interpass times and the total rolling times are short, is not conducive for extensive precipitation. It is, therefore, not unreasonable to assume that Nb will influence the behavior of austenite first as a solute and then as a precipitate in plate and structural rolling, whereas it is expected that Nb would largely remain in solid solution during strip and bar rolling [93,103].

Behavior of Niobium in Austenite

When a Nb-bearing low-alloy steel is in the austenite phase field, the Nb will be in both the solid solution matrix and in the precipitated NbCN, the partitioning depending on temperature. At equilibrium, this partitioning of Nb between the matrix and precipitate will be controlled by the solubility relations discussed earlier. Since one of the primary requisites of a successfully conditioned austenite is the presence of a large number of crystalline defects that can act as sites for ferrite nucleation during cooling, i.e., a total near-planar crystalline defect surface or boundary area per volume (S_v), the motion of subgrain and grain boundaries associated with static recrystallization and grain growth after hot deformation must be retarded. Evidence for this retardation by Nb in both solid solution [104-106] and in precipitate [107-109] can be found in the literature.

The different effects of NbCN precipitation during hot rolling have stimulated a large number of studies concerned with the kinetics of precipitation in austenite as influenced by composition, strain, strain-rate, temperature and overall heat treatment. This group of studies of precipitation kinetics has utilized a wide variety of techniques including: chemical analysis [10,12,29,51,110,111], electrical resistivity [111,112], X-ray diffraction [84], quantitative electron microscopy [86], flow curves [106], and hardness testing [111,113,114]. The precipitation which has been studied in these experiments is, with one exception, the strain-induced precipitation which occurs during and/or after deformation. The exception is the dynamic precipitation which accompanies deformation and which has been studied by Jones and Rothwell [108] and Akben et al. [115].

Studies of the precipitation in recrystallized austenite have shown that the kinetics are very sluggish [9,104,111,112]. The results of the study by Simoneau et al. [111] on precipitation rates at temperatures above 900°C are shown in Figure 14. The kinetics of NbCN precipitation at 900°C is shown in Figure 15; these data are from the work of LeBon et al. [104]. Finally, the precipitation kinetics at low temperatures, below 950°C, has also been determined by Watanabe et al. [9]; these results are shown in Figure 16. These studies illustrate the slow rate of precipitation in recrystallized austenite; it takes several thousands of seconds at 900°C for 50 percent of the potential precipitates to form. Also, by combining the results of Simoneau et al. [111] and Watanabe et al. [9] the overall precipitation behavior does appear to conform to C-curve kinetics.

The precipitation rate is remarkably sensitive to the level of strain imparted prior to aging, as is illustrated by the results of LeBon et al. [104], Figure 15, and Hoogendorn and Spanraft [53], Figure 17. The strain-induced precipitation of NbCN in austenite appears to follow C-curve kinetics. Three C-curves, each based on a different technique, are shown in Figures 17-19. These results are from the work of Watanabe et al. [9], Figure 16; Ouchi et al. [113], Figure 18; and Hansen et al. [86], Figure 19. In all three cases, the nose of the C-curve appears to be in the temperature range 900 to 950°C.

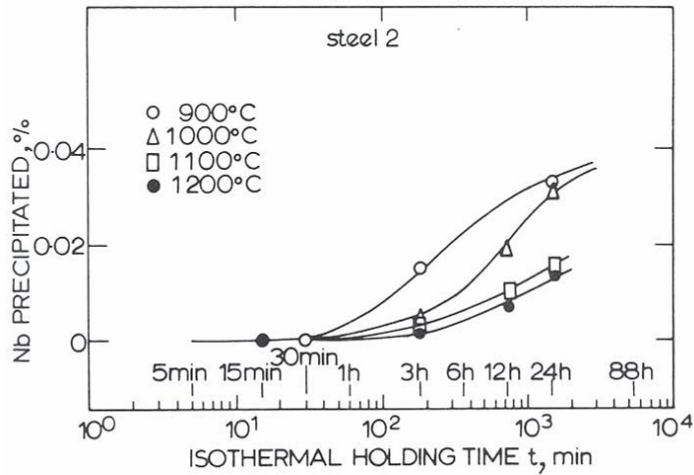


Figure 14. Isothermal precipitation of Nb in undeformed austenite in steel containing 0.07%C-0.04%Nb-0.010%N [111].

The overall composition of the steel appears to have a strong effect on the kinetics of precipitation [9,106,114]. For example, the presence of Mo appears to shift the C-curve to lower temperatures and shorter times [9], whereas an increase in Mn level acts to shift the C-curve to longer times [115]. These effects are probably caused by the influence of these elements on the activities of solute Nb and C, as discussed above.

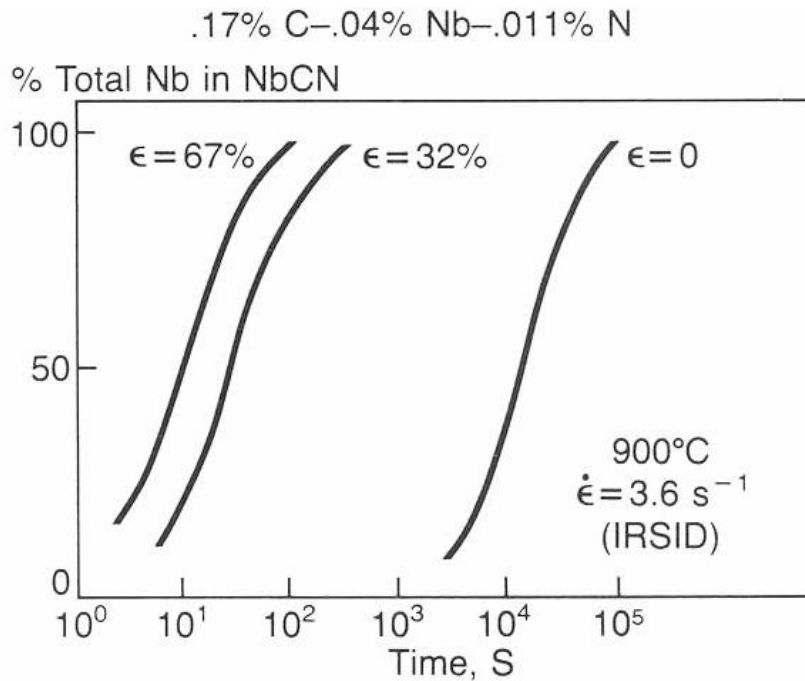


Figure 15. Influence of strain level on the kinetics of Nb precipitation at 900°C [104].

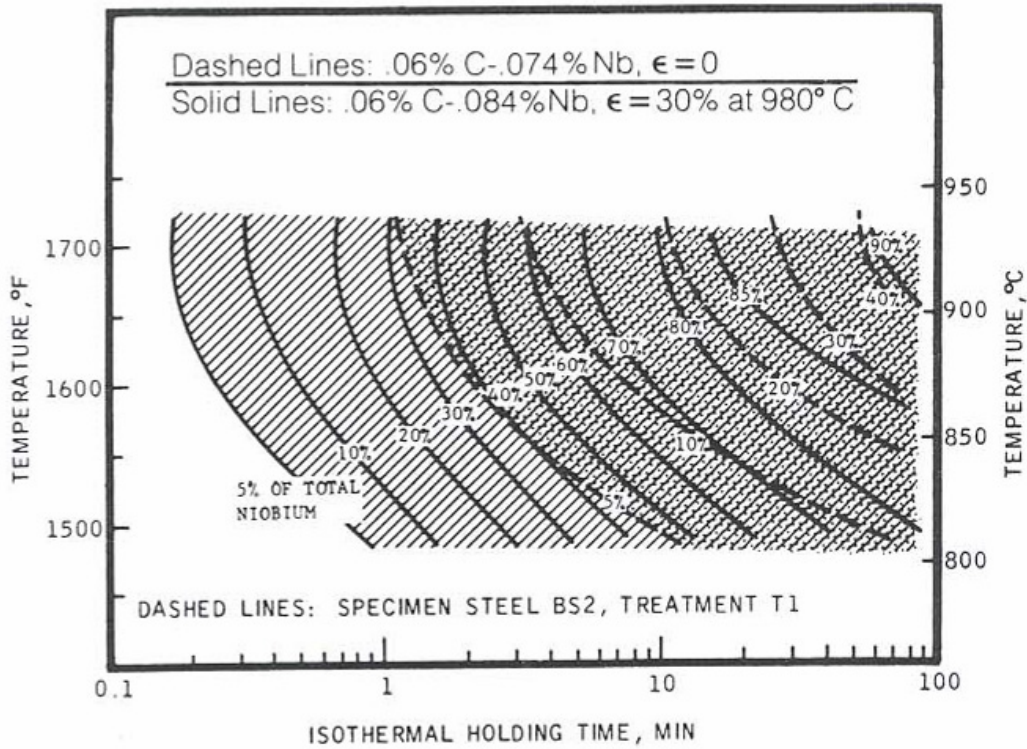


Figure 16. Time-temperature-precipitation diagram showing effect of deformation of Nb(C,N) in austenite [9].

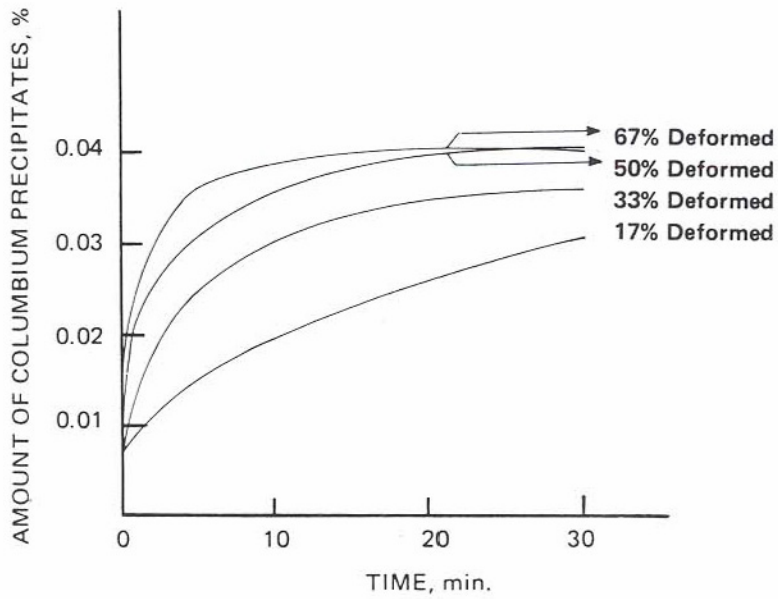


Figure 17. Influence of deformation on precipitation in a steel containing 0.06%C-0.041%Nb and 0.06%N [53].

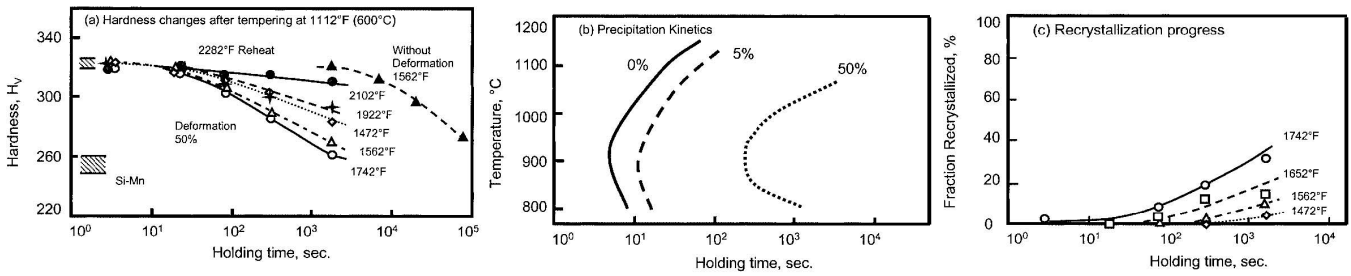


Figure 18. Precipitation of Nb(CN) and recrystallization kinetics during isothermal holding in Nb-bearing steel, (a) hardness changes after tempering at 600°C, (b) precipitation kinetics and (c) recrystallization progress [113].

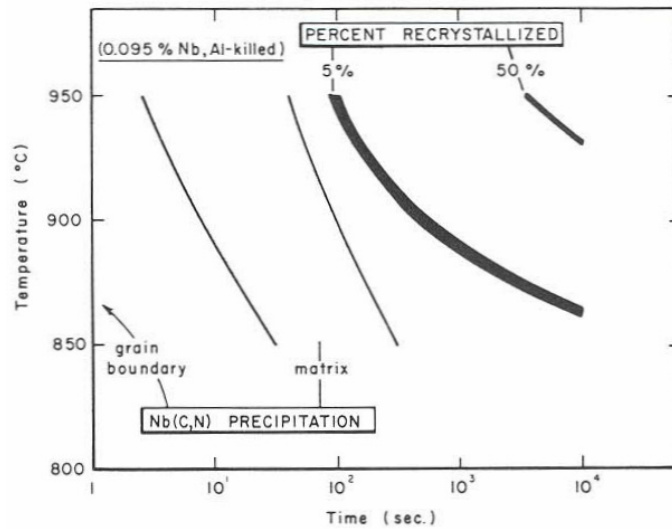


Figure 19. Recrystallization-precipitation-temperature-time (RPTT) diagram for steel 3 after solutionizing at 1250°C and hot rolling 50% at 950°C [86].

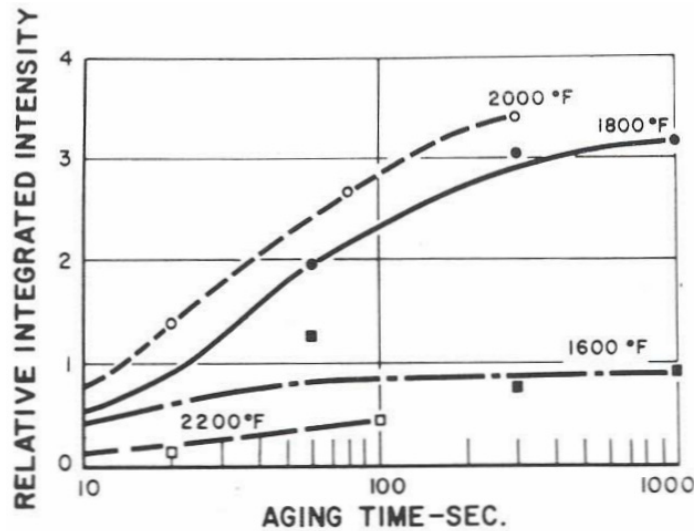


Figure 20. Relative integrated intensity versus aging time for samples deformed 60% at the indicated temperatures [84].

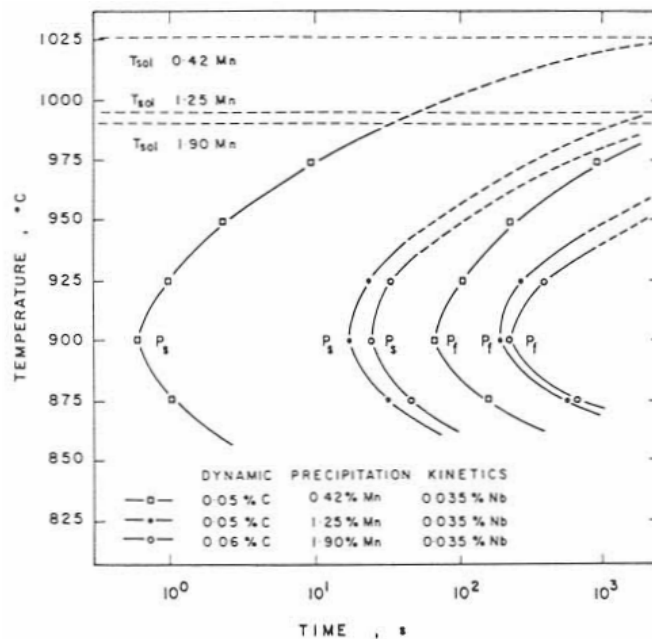


Figure 21. PTT curves for dynamic precipitation of NbCN in austenite [115].

Studies of the precipitation of NbCN in deformed austenite are subject to certain problems when the temperatures of deformation (and subsequent holding) are raised. The problem arises because the density of crystalline defects in the austenite does not vary continuously with temperature over a large temperature range, say, $800 \leq T \leq 1200^\circ\text{C}$. For a given set of conditions of composition, temperature, strain and strain-rate, the austenite deformed at high temperatures may experience static recrystallization between passes if the interpass time is sufficiently long. This would be expected at large strains, high temperatures and high strain rates. The austenite grain structure deformed at low temperatures will be highly elongated and the austenite deformed at intermediate temperatures will have a mixed equiaxed plus elongated grain structure. Behavior of this kind would be expected to give a discontinuous relationship between the crystalline defect density that can act as nucleating sites for NbCN precipitation and the deformation temperature. This type of austenite deformation behavior has been observed in microalloyed steels [32,84] and has been shown to influence the results of precipitation kinetic studies [86]. An example of this effect is shown in Figure 20, which has been taken from the work of Davenport et al. [84], Figure 20, where the relative integrated intensity from NbC diffraction peaks is assumed to be roughly proportional to the volume fraction of precipitate, indicates that there are high rates of precipitation in the temperature range 950 to 1100°C and lower rates at temperatures which are either above or below this range. Davenport et al. [84], have noted that the lowering of precipitation kinetics which results from higher temperature deformation and holding may be due to two effects. The first is the reduction in solute supersaturation with increasing temperature; this alone would lead to a decrease in precipitation rate. The second is the change in deformation structure of the austenite near 1100°C. Austenite rolled below this temperature leaves the rolls with an elongated, deformed microstructure that contains numerous sites for strain-induced precipitation. Austenite rolled above this temperature quickly achieves the statically recrystallized state; this structure contains few sites for strain-induced precipitation; hence, low precipitation kinetics can be expected.

The studies of precipitation kinetics described to this point have involved “static” precipitation. That is, the austenite has been deformed in one operation and then aged in a second operation.

A different approach to studying strain-induced precipitation has been developed by Jonas et al.

[106,115]. This approach enables the kinetics of strain-induced precipitates to be determined in a “dynamic” context, i.e. where the austenite is being strained and aged at the same time. This approach yields C-curves describing the dynamic precipitation and is based on the analysis of hot flow curves. C-curves describing this dynamic precipitation [115] are shown in Figure 21.

Principles of Austenite Conditioning

There are two different approaches available for austenite conditioning during hot rolling. They are known as conventional controlled rolling (CCR) and recrystallization controlled rolling (RCR). The purpose of this paper is to describe these practices, to show how they differ from conventional hot rolling (CHR), and to indicate the microalloying additions required for their respective implementation [93,103,116]. In addition, the requirements of the mill equipment suitable for these practices will be discussed.

Conditioning of Austenite

Obtaining fine ferrite grain sizes from the transformation of austenite requires high rates of ferrite nucleation, and low rates of growth and subsequent coarsening. Conditioning of austenite means that the microstructure of the austenite has achieved, through controlled hot deformation, the proper predetermined metallurgical state or condition prior to transformation that will embody these requirements. It was shown earlier that high ferrite nucleation rates result from having a large number of potential nucleation sites and a high nucleation rate per site [92,117,118]. The sites for ferrite nucleation are austenite grains and incoherent twin boundaries and deformation bands [92,119-124]. The density of these sites per unit volume is expressed as the total interfacial area of the near-planar boundaries per unit volume and has the units mm^2/mm^3 or mm^{-1} . This stereological concept was first discussed by Underwood [125], and was later adopted to describe austenite by Kozasu et al. in 'Microalloying' 75 [119]. Kozasu et al. called this measure of the total interfacial area per unit volume, the parameter S_v . The parameter S_v can be considered as an approximate austenite “grain size”, and its magnitude is an indication of the degree of austenite conditioning. The principal goal of TMP and austenite conditioning is to maximize S_v . The influence of S_v on ferrite grain size is shown in Figure 22 [126].

There are two entirely different approaches to increasing S_v . In the first, the initially recrystallized reheated austenite grains undergo repeated recrystallization during subsequent hot deformation leading to grain refinement. This deformation would take place at temperatures above T_{95} in Figure 23. Here, one set of equiaxed grains is replaced by a new set of finer, equiaxed grains. Since these fine grains would have a strong tendency to coarsen during the interpass time, this fine grain size can be retained only if a suitable mechanism is available to suppress grain coarsening. The process that involves repeated recrystallization and inhibition of grain coarsening is called Recrystallization Controlled Rolling (RCR), and was originally proposed by Sekine et al. [127,128]. Clearly, the lower the T_{95} , the larger will be the processing window between the reheat temperature and the minimum finishing temperature of T_{95} . Hence, steels designed for RCR conditioning must have a low recrystallization-stop temperature and a pre-existing grain coarsening inhibition system. This practice is well-suited for production conditions that require high finishing temperatures, e.g. underpowered rolling mills, heavy section and heavy plate rolling, and forging.

The second approach involves substantial deformation below T_5 , where, for example, the thickness at T_5 is three or four times the final gauge. In this method, the grain size at T_5 is deformed and stays unrecrystallized through the interpass time for all subsequent passes. Hence, there is a change in grain shape and the occurrence of transgranular twins and deformation bands. The process that involves

repeated flattening or "cold working" of the grains by repeated deformation below T_5 is called Conventional Controlled Rolling (CCR). Clearly, the higher the T_5 the more passes can be used and the more effective is the practice. Hence, steels designed for CCR conditioning must have a high recrystallization-stop temperature.

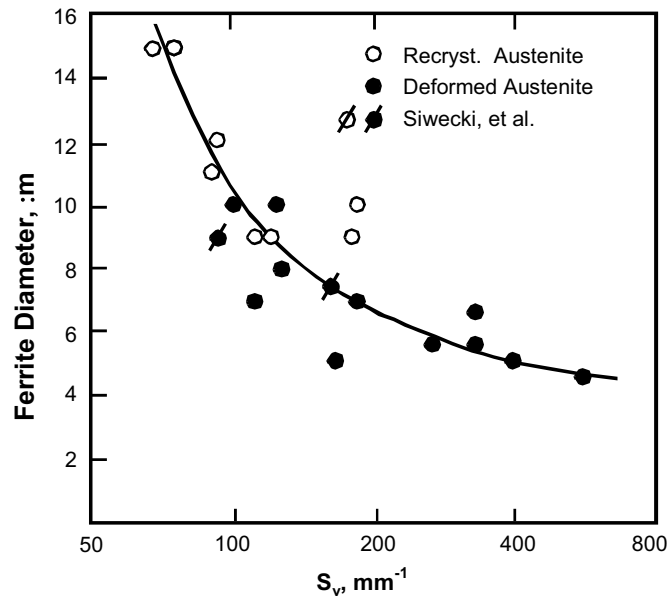


Figure 22. Ferrite grain sizes produced from recrystallized and unrecrystallized austenite at various S_v values [126].

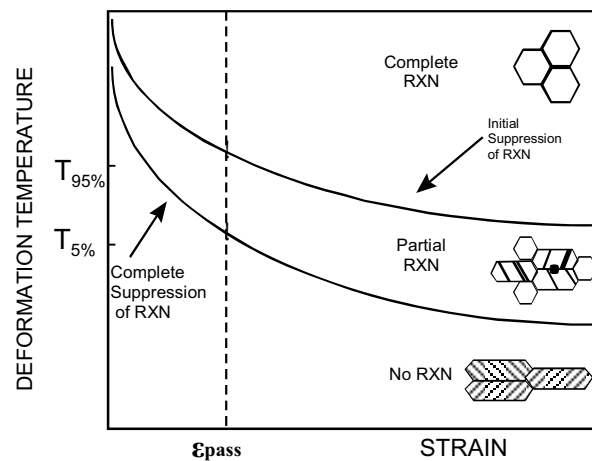


Figure 23. Schematic illustration of austenite microstructures resulting from various deformation conditions [36].

Although there are two different approaches to austenite conditioning, i.e. RCR and CCR, they both have the same objective of resulting in structural refinement in the final plate, coil, beam, or forging. The differences between RCR and CCR can be easily understood with the aid of Figure 24, which shows the different paths used by each to achieve high values of S_v [129].

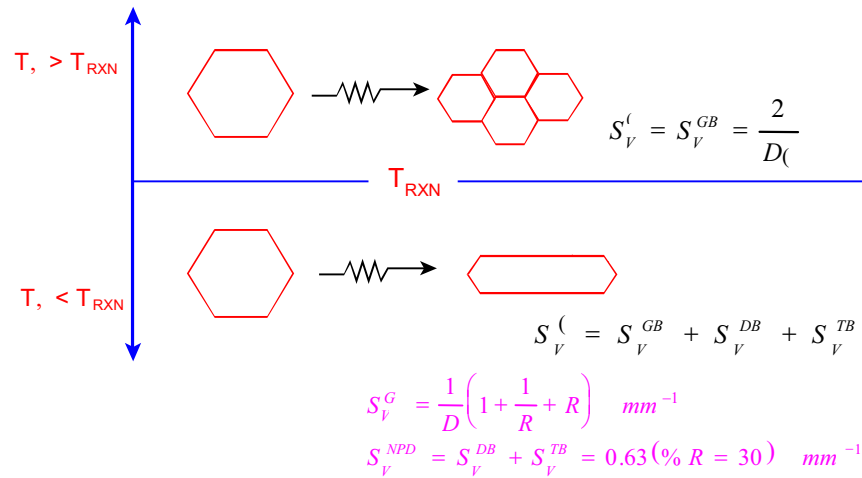


Figure 24. Schematic representation of austenite microstructure when deformed above or below the recrystallization-stop temperature of austenite, with corresponding description of S_v . Note that the superscripts GB, DB, TB and NPD denote the contribution to the total S_v from grain boundaries, deformation bands, twin boundaries and near planar defects [129].

The increase in S_v for the RCR practice comes exclusively from the increase in grain boundary area per unit volume which results from a decrease in average grain volume, while the increase in S_v for the CCR practice results from the increase in grain boundary area per unit volume resulting from a change in grain shape and through the addition of the transgranular twins and deformation bands.

Role of Niobium in Thermomechanical Processing

The value of an alloying or microalloying addition to a steel from an austenite conditioning standpoint for controlled rolling derives from its ability to generate sufficiently large pinning forces to retard the motion of crystalline defects such as dislocations, sub-grain boundaries and grain boundaries during recovery and recrystallization, that would otherwise occur to lower the free energy of the system. Hence we are interested in a quantitative assessment of how a given addition can retard recovery and recrystallization. This is accomplished through the use of the well-known, so-called “double hit test” [64,130-132], where a series of samples is reheated to a given temperature and then cooled to the temperature of interest. One specimen is deformed continuously to a large strain and the resulting flow curve acts as a reference for the interrupted tests to follow. Other specimens are deformed to a constant pre-strain, often approximating a rolling pass strain, after which they are unloaded, held at temperature for various delay times, then reloaded past yielding. Some measure of softening is recorded for each holding time and plots of fractional softening versus holding time at a given temperature are constructed [64,130-132]. Earlier work on austenite has shown, approximately, that the initial 25% softening is caused by static recovery while the remaining 75% is due to recrystallization [64,130].

This technique has been used in numerous previous studies [64,130-132], and Nb has repeatedly been shown to strongly retard the progression of both recovery and recrystallization of austenite [36,64,130,133]. An example of the retarding effect of solute Nb is shown in Figure 25 taken from the work of Yamamoto et al. [134].

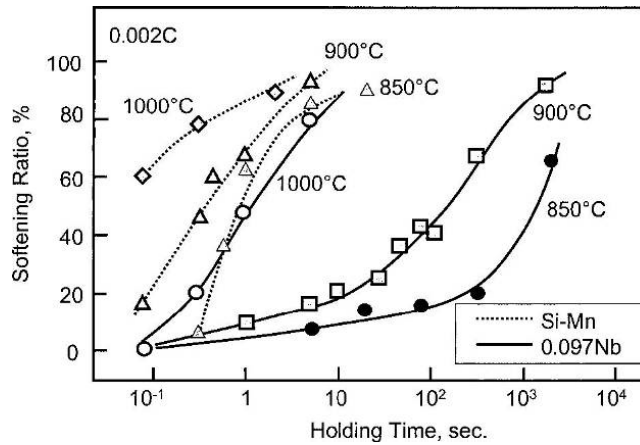


Figure 25. The effect of deformation temperature on the softening behavior in 0.002C and 0.002C-0.097Nb steels [134].

In the experiment leading to Figure 25, the Nb is assumed to be in solution in the austenite. Hence, the solute Nb was responsible for delaying the onset of recrystallization at 850°C from 20 sec in plain carbon steel to 400 sec in the Nb steel for a true pre-strain of 0.69 applied at a strain rate of 10 per sec. A comparison of the solute retarding effects of the three microalloying elements Nb, Ti and V is shown in Figure 26 [134]. It is obvious that V has the weakest retarding effect, with Ti intermediate and Nb the strongest. It is also clear that the behavior exhibited in Figure 27 represents the same trend as found in the Cuddy diagram, Figure 27 [135].

A comparison of the relative retarding effects of Nb as a solute and as a precipitate is shown in Figure 28 [134]. In Figure 28, the Nb in the steel with 0.002C is in solution whereas the Nb in the steel with 0.019C is present as precipitates. The precipitation has caused an order of magnitude longer delay for the onset of recrystallization and an even much larger retardation in the progress or rate of recrystallization.

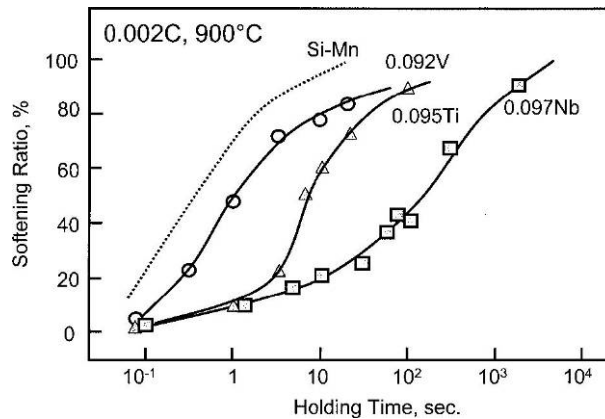


Figure 26. The comparison of Nb, V, and Ti effect on the softening behavior in 0.002C steels [134].

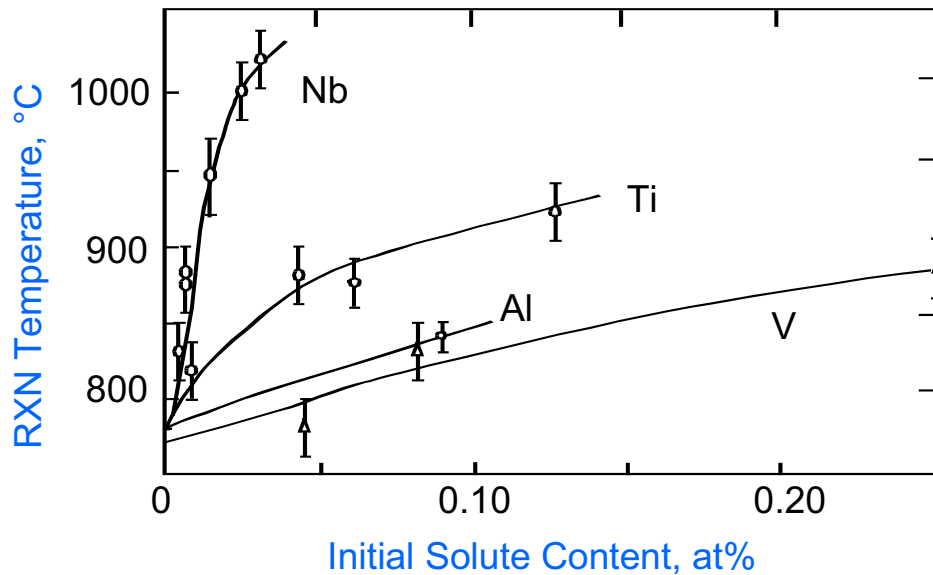


Figure 27. The increase in recrystallization temperature with increase in the level of microalloy solutes in a 0.07C, 1.40Mn, 0.25Si steel [135].

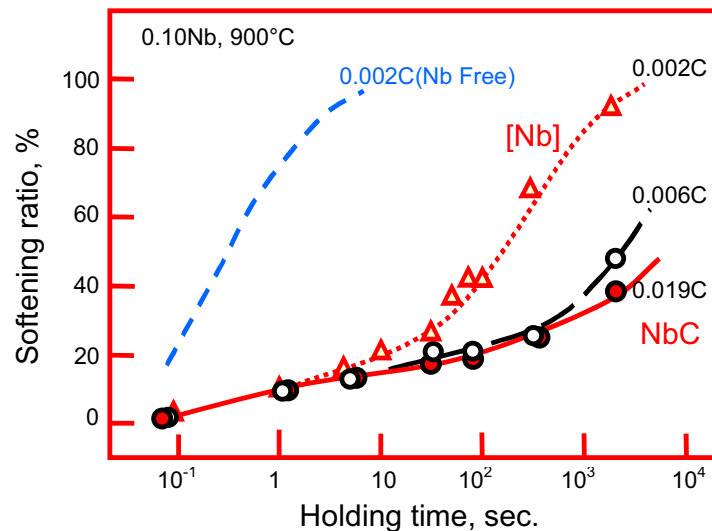


Figure 28. The effect of C content on the softening behavior in 0.10 Nb steels at 900°C [134].

A somewhat different example of this softening behavior is shown in Figure 29 [130] where the behavior of three steels is compared. The difference in the nature and magnitude of the influence of solute Nb and precipitated Nb is clear in Figure 29. The arrows shown in Figure 29 denote the earliest appearance of strain-induced precipitation in austenite. Solute Nb is capable of suppressing recrystallization for short times while precipitated Nb can for much longer times. Hence, either solute or precipitated Nb would be expected to suppress recrystallization in strip mill rolling which has short interpass times, while solute Nb alone could not in a reversing plate mill with much longer interpass times. In this case, precipitated Nb would be needed.

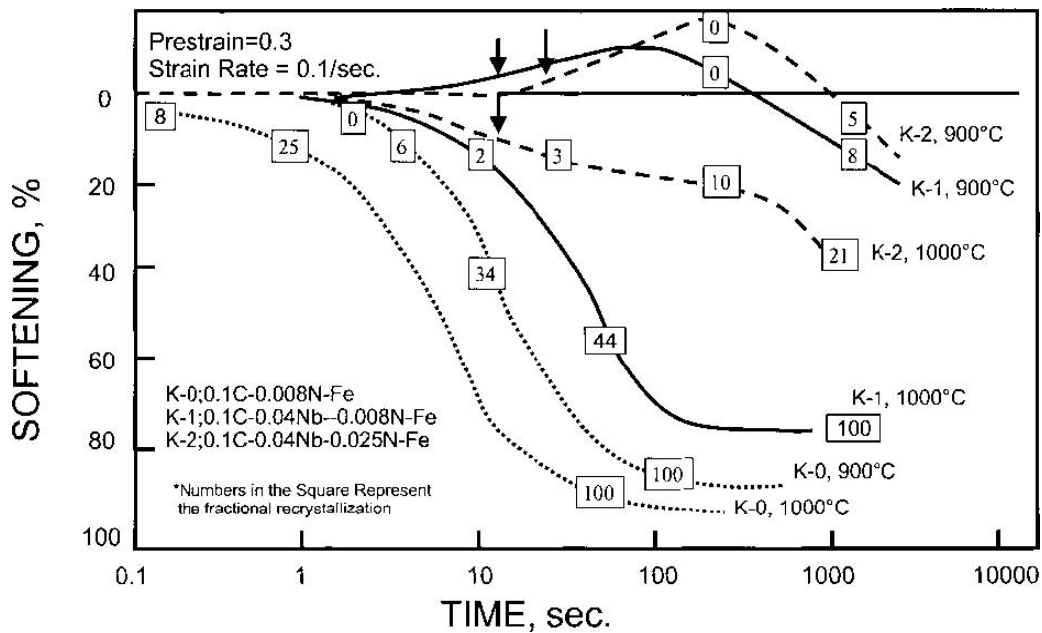


Figure 29. Static restoration behavior of three steels at 900°C and 1000°C. Arrows denote first observable precipitation [130].

When a deformed, supersaturated solid solution of Nb in austenite is held at different temperatures, there is a competition concerning kinetics between precipitation and recrystallization and their interaction. Several studies have attempted to treat this rather complex situation [106]. One example of such work is shown in Figure 30 [130], where the behavior of plain carbon steel is compared to that of a Nb steel.

In an attempt to explain the behavior shown in Figure 27, Cuddy tried to calculate the pinning force required by NbC particles to suppress recrystallization [135]. This was done by equating the driving force for recrystallization with pinning force generated by the particles. In Cuddy's work, the volume fractions required for the pinning force estimate were calculated using published solubility equations. He found that the assumed homogeneously distributed array of particles could suppress recrystallization. In later work, Palmiere et al., conducted a similar experiment but where the characteristics of the precipitate array were taken from experimental observations [64]. This work differed from Cuddy's in one important way. In the study by Palmiere et al., real and local volume fractions and particle sizes were measured on austenite grain and subgrain boundaries and in the grain interiors. The pinning forces that resulted from these observations showed that the forces calculated at the grain boundaries were well in excess of the driving force and could easily be responsible for the observed suppression of recrystallization. These results are summarized in Figure 31 [6].

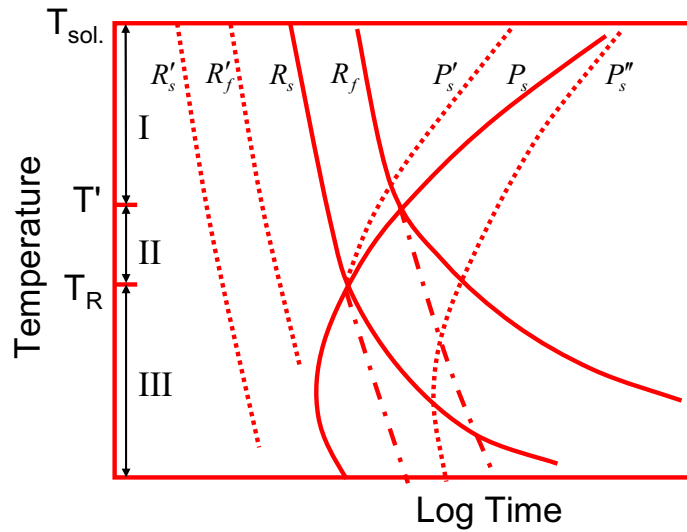


Figure 30. RPTT diagram showing the interaction between precipitation and recrystallization. R_s and R_f refer to the start and finish of recrystallization, respectively, in HSLA steels; and R'_s and R'_f refer to the start and finish of recrystallization, respectively, in plain carbon steels. P_s and P''_s refer to the hypothetical precipitation-start times in deformed and undeformed austenite, respectively. P_s is the actual precipitation-start time [130].

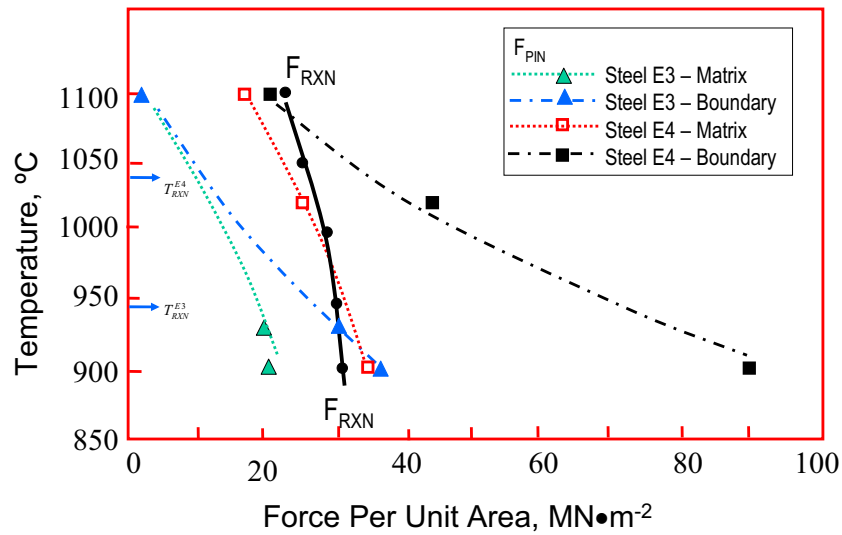


Figure 31. Comparison between F_{PIN} and F_{RXN} versus deformation temperature. Data to the right of F_{RXN} will result in the complete suppression of austenite recrystallization. Data to the left of F_{RXN} will result in a partial or fully recrystallized austenite microstructure [64].

While it is now possible to explain why the Nb in the Cuddy diagram behaves the way it does, Figure 27 [135], i.e., that the recrystallization stop temperature increases strongly with increasing bulk Nb content, what remains to be explained is why the microalloying elements differ in effectiveness from one another. One possible explanation is given in Figure 32 [133], where the temperature dependence of the driving force for precipitation, i.e., the supersaturation, is plotted versus temperature for various microalloying precipitating systems. Of all the possible precipitating systems, only NbC can have high supersaturations over a large portion of the typical hot rolling temperature range [64].

Transformation and Strengthening in Nb Steels

Niobium and Transformation of Austenite

What is presented here are the manifestations of Nb beyond, and in opposition to, the ferrite grain refining effects attributed to the austenite conditioning described above. The high S_v that results from controlled rolling by itself would lower the hardenability of the austenite. In order to obtain lower transformation temperatures and low temperature transformation products, this effect must be overcome by a combination of higher alloying and/or accelerated cooling. When relatively large amounts of Nb are in solution in austenite at the transformation temperature, i.e., high Nb contents, low C contents, and high reheating temperatures, it often has an important effect on the CCT diagram and subsequent transformation during continuous cooling. This is manifested as both lower transformation start temperatures and a higher probability of achieving non-polygonal ferrite microstructures, especially at higher cooling rates. The first effect was reviewed earlier [7,53,110,136,137], and a good example is shown in Figure 33 [138].

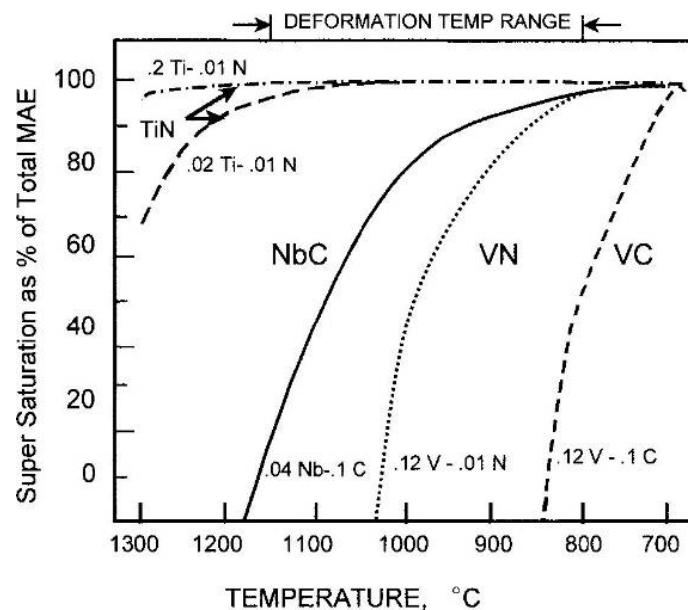


Figure 32. Precipitation potential of various microalloying systems [133].

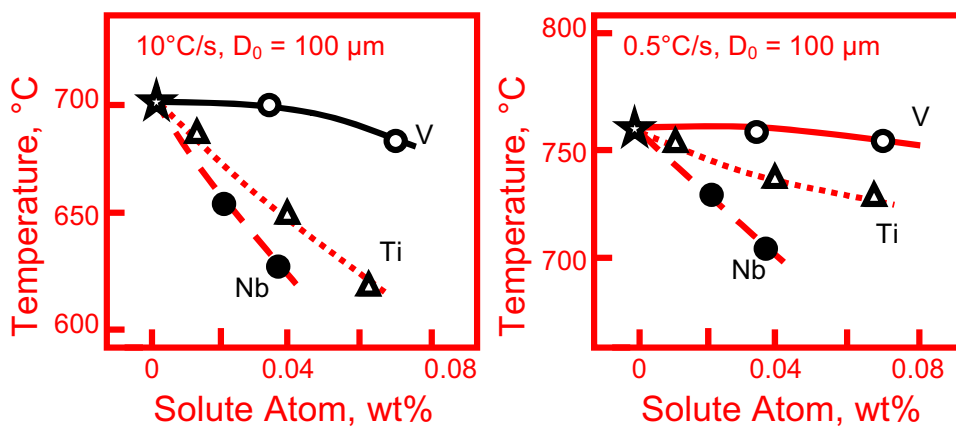


Figure 33. Corrected A_{3} temperatures of microalloyed steels with standard austenite grain size of $100 \mu\text{m}$ [138].

More recent work has shown that more than just the temperature is altered by solute Nb. The increase in hardenability also means that for the same general conditions, the Nb steels will exhibit larger amounts of low temperature transformation products such as acicular ferrite, Widmanstatten ferrite and bainitic ferrite, particularly at higher cooling rates [138,139]. An example of this effect is shown in Figure 34 [138].

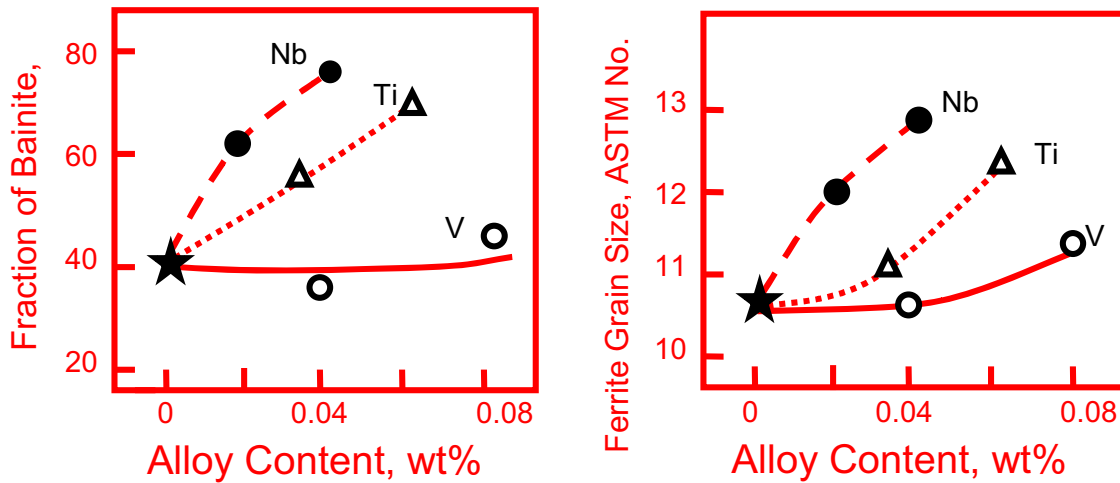


Figure 34. Effects of Nb, V and Ti on volume fraction of bainite and ferrite grain size in accelerated cooled steels [138].

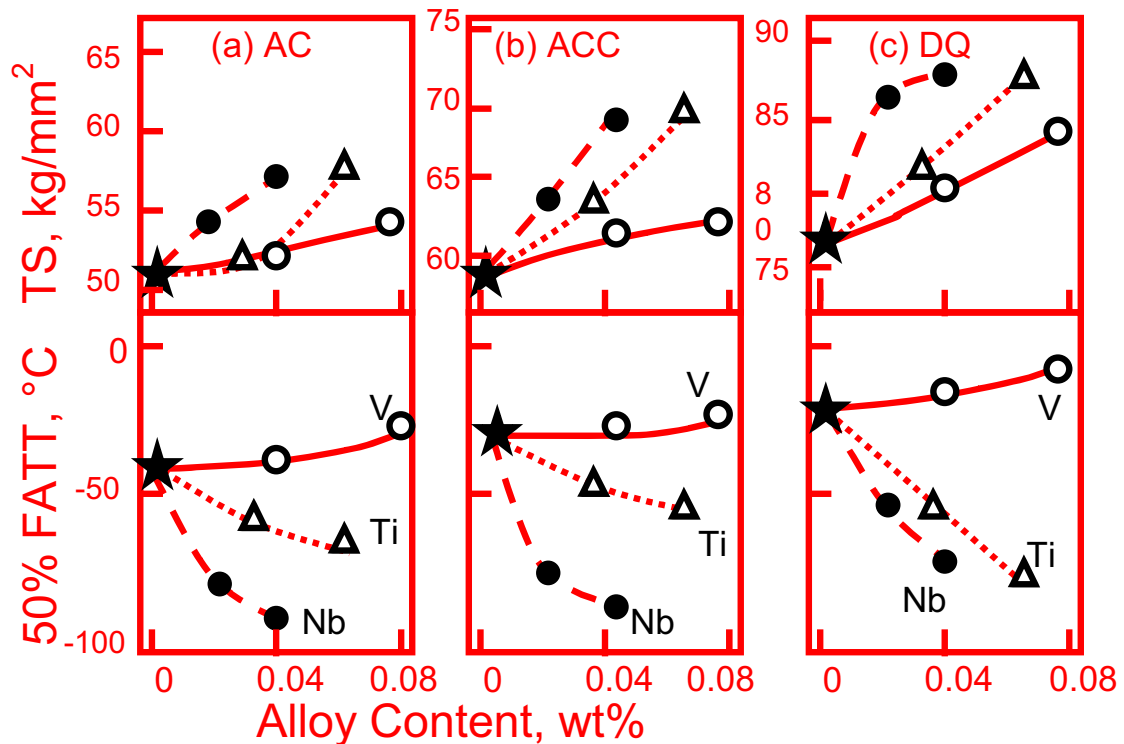


Figure 35. Effects of addition of Nb, V and Ti on tensile strength and Charpy V 50% FATT of (a) air cooled, (b) accelerated cooled and (c) direct quenched steels after controlled rolling [138].

What is particularly striking about the effects shown in Figures 33 and 34 is the influence on properties, Figure 35 [138]. While it is true that the Nb addition had a strong effect on ferrite grain size, Figure 34, the principal effect was on the nature of the ferrite. At 0.04 Nb, about 80% of the ferrite was bainitic, Figure 34. It seems obvious from Figure 35 that the strength increased directly with the amount of bainite. Several similar examples have been also shown elsewhere [140-144]. The question then arises as to how the solute Nb is responsible for the improvement in FATT. Is it the grain refinement of 20% of the structure that is polygonal ferrite? Or, is it the presence of low carbon bainite? In simple terms, this effect on toughness is likely due to the Nb acting as both a hardenability agent and as a grain refiner.

The transformation products resulting from the decomposition of austenite containing Nb as a solute have a surprisingly high dislocation density. This was to be expected for acicular ferrite and bainite, which, by their nature, exhibit very high dislocation densities [141,142]. What was not expected was the rather high dislocation densities found in what is usually called polygonal ferrite in Nb steels [140,141,145-147]. This often overlooked characteristic of Nb steels has very important ramifications regarding mechanical properties as will be shown below.

Niobium and Strengthening

There is no doubt that the addition of Nb to most low alloy steels results in higher yield strengths. This is true for both plate and strip products. What remains elusive is the precise way that Nb causes this effect. The analysis of strength usually starts with the expanded Hall-Petch equation, where a linear additivity of strength components is assumed:

$$Y_{S_{obs}} = [Y_{S_{P-N}} + \Delta Y_{S_{SS}} + \Delta Y_{S_{Texture}} + \Delta Y_{S_{disl}}] + \Delta Y_{S_{pptn}} + k_y D_\alpha^{-1/2} \quad (18)$$

where:

$Y_{S_{obs}}$	=	observed yield strength
$Y_{S_{P-N}}$	=	lattice friction stress
$\Delta Y_{S_{SS}}$	=	stress increment caused by solid solution
$\Delta Y_{S_{texture}}$	=	stress increment caused by texture
$\Delta Y_{S_{disl}}$	=	stress increment caused by dislocation
$\Delta Y_{S_{pptn}}$	=	stress increment caused by precipitation
$k_y D_\alpha^{-1/2}$	=	contribution by the ferrite grain size

The universal use of this equation has been questioned lately from several perspectives. First, the general accuracy of this approach has been questioned and new summation approaches have been suggested [148-152]. It appears that the linear additivity approach sometimes overestimates the observed yield strength, and other means of summing such as a root-mean-square summation might be more appropriate [148-151]. However, a recent study of several 350 grade strip steels containing Nb showed that the linear approach was reasonably accurate [145,146,153]. Second, if the equation is inaccurate or invalid, then its use may lead to erroneous interpretations as to how Nb actually strengthens ferrite. For example, the precipitation hardening increment has often been determined in the literature by subtracting all other components from the measured yield strength. Clearly, this would lead to incorrect values of precipitation hardening if the linear summation law were incorrect or inappropriate.

What follows are some of the potential problems encountered in ascribing attributes to Nb in terms of contributions to strength. Consider the contribution caused by grain refinement when what is taken to be polygonal ferrite is formed at decreasing transformation temperatures, e.g., as a result of accelerated

cooling in a controlled rolled Nb steel that still has a portion of the initial Nb remaining in solution. While there is little doubt that there is a reduction in ferrite grain size with falling transformation temperature, there is also a subtle change in both the nature of the ferrite and in the grain boundaries [147]. As the transformation temperature decreases, the grains become more irregular in shape and boundary rugosity, and a higher proportion of the grain boundaries assume a lower angle character. Hence, it seems most unlikely that the same Hall-Petch slope would be valid for both high angle grain boundaries found in the larger polygonal ferrite formed at higher transformation temperatures and low angle grain boundaries found in the smaller non-polygonal ferrite formed at the lower temperatures. This would lead to an over-estimation of the contribution of grain size to strength at lower transformation temperatures.

The precipitation of NbC in ferrite is often taken to be a major contributor to the strength of ferrite. While this is widely assumed to be the case, there is very little direct evidence that any observed precipitation actually results in significant amounts of precipitation hardening of ferrite by NbC that occurs in commercial Nb steels, particularly strip steels. There are good reasons for this lack of evidence. First, the NbC lattice does not fit particularly well in either austenite or ferrite, as was shown by the lattice misfit strain in Table IV. This means that all precipitation will be either semi-coherent or incoherent with the matrix, and will require crystalline defects such as dislocations, deformation bands, or subgrain and grain boundaries to aid in the nucleation.

As mentioned earlier, there have been two types of precipitation formed in ferrite in transformed microalloyed steel: interphase and general. Interphase precipitation forms in the ferrite at the advancing austenite-ferrite interface as the transformation occurs. This leads to a sheet-like distribution where the carbides exhibit only one of the three possible variants of the Baker-Nutting orientation relationship [72,73,87,154,155]. Importantly, interphase precipitation of NbC is usually found in ferrite formed at temperatures above 700°C. General precipitation forms from a supersaturated low temperature acicular or bainitic ferrite after the completion of the transformation, i.e., a form of direct aging. General precipitation exhibits all three of the variants of the Baker-Nutting orientation relationship [154,155]. Examples of interphase and general precipitation are shown in Figures 12 and 13 [13]. The formation of interphase precipitation has been studied in Nb steels [155-157], and its occurrence is shown in the TTT diagram of Figure 36 [155-157] for a steel containing 0.07C-1.07 Mn -0.033Nb. These results were later verified by Thillou et al. in a steel containing 0.08C-1.3Mn-0.025Nb [145,146].

It is immediately apparent from Figure 36 [155-157], that only very specific thermal paths will intersect the precipitation region, even after it is converted to a CCT diagram. For example, the chances of encountering interphase NbC in a commercial strip product seem highly unlikely, given that the strip would be water spray-cooled at 30-80 °C/sec to around 650-600°C and then very slowly cooled to room temperature. This cooling path would completely miss the region of the TTT or CCT diagram for interphase precipitation, i.e., temperatures in excess of 700°C. Similarly, the accelerated cooling of plate at 10 °C/sec to around 600° C or below, followed by air cooling, would also be expected to largely miss this region on the TTT diagram. However, the air cooling of plate at below 1 °C/sec from the finish rolling temperature might be expected to penetrate the interphase region. Sakuma and Honeycombe have suggested that the prerequisite for the formation of interphase precipitate is a balance between the ferrite growth rate and the supersaturation of NbC in ferrite [155-157]. Interphase precipitation is favored by slow growth rates and high supersaturations of NbC. It is quite important to note that little general precipitation was found below 700°C in the Sakuma and Honeycombe study. Again, this was also found by Thillou et al. [145,146]. In a similar vein, little precipitation hardening was found in studies of both laboratory processed (i.e., coiled) and commercial 350 grade Nb high strength strip [145,146].

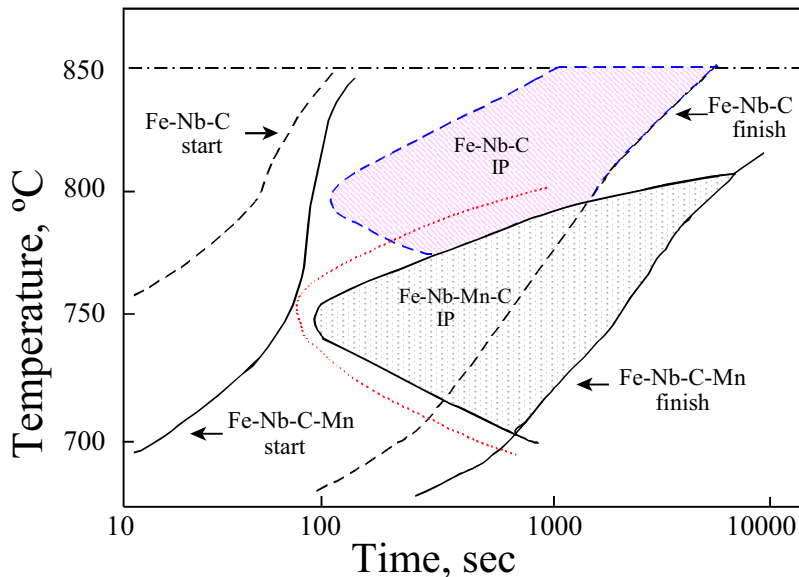


Figure 36. Schematic TTT curves for Fe-0.036Nb-0.09C and Fe-0.036Nb-0.09C-1.07Mn alloys; interphase precipitation (IP) occurs in certain shaded areas. Combined data from Sakuma and Honeycombe (1985) [155-157] and V. Thillou et al. (1998, 0.28Nb-0.07C-1.1Mn, dotted line).

These observations regarding precipitation in strip steels are important, but it should be kept in mind that the Nb levels used in these steels were 0.035% or less. It is interesting to consider what might be expected in steels of higher Nb content and where the Nb/C ratio is closer to stoichiometry, which would maximize the volume fraction of NbC available for precipitation. In this regard, TEM studies of commercial strip steels containing 0.09C-1.2Mn-0.1Nb [87] and 0.08C-1Mn-0.065Nb [158] revealed that little, if any, fine scale precipitate was present in either steel. On the other hand, a recent TEM study of a high Nb plate steel designed for high temperature processing, designated HTP steel, containing 0.03C-1.5Mn-0.08Nb and air cooled to room temperature after rolling, revealed that precipitation in ferrite representing approximately 80 MPa of Orowan-Ashby strengthening was found [159]. Also, precipitation hardening approaching 100 MPa has been found in air cooled plate containing 0.04 Nb and a ferrite-pearlite microstructure that exhibited a yield strength of 450 MPa [160]. These values of 80-100 MPa probably represent the maximum amount of real precipitation hardening achievable in Nb steels with normal compositions and processing.

It is interesting to note that the magnitude of precipitation hardening found in the plate steels, i.e., 80-100 MPa, is fairly closely predicted by two diagrams representing precipitation hardening according to the Orowan-Ashby theory. If one assumes (i) particle diameters of 2-3 nm and (ii) that perhaps 50-70% of the bulk Nb might be available after rolling for precipitation in the ferrite, then the diagrams published by Gladman et al. [161] and Gray [162] predict values of precipitation hardening fairly close to the values quoted for the air cooled plate steels. However, it is extremely important to mention that the values predicted by these diagrams are maximum values that require certain special processing conditions for a given level of Nb to achieve its full precipitation hardening potential. The simple presence of Nb in a steel clearly does not guarantee any level of precipitation hardening.

By the early 1980's, it was well known that the structure and properties of polygonal ferrite steels had been fully optimized. For example, precipitation hardened, controlled rolled and air cooled low carbon ferrite-pearlite steels containing 0.04 Nb, and less than 1.5% Mn and with a ferrite grain size of 5

microns could be expected to exhibit a yield strength of around 400-420 MPa in strip and light plate. However, with the passage of time, technological applications were demanding even higher strength levels. It was clear that other approaches to microstructural design were needed to reach yield strengths over 450 MPa, while keeping other important properties at acceptable levels.

One of the largest changes in the steel metallurgical landscape in the last twenty years is the application of multi-phase microstructures in both strip and plate products. Multi-phase steels include dual-phase (ferrite-martensite-retained austenite) [163-165] and transformation-induced plasticity (TRIP) steels (ferrite-bainite-retained austenite) [166,167]. While ferrite-pearlite microstructures can reach yield and tensile strengths of 420 and 550 MPa, respectively, the multi-phase steels can reach tensile strengths well in excess of 600 MPa. Neither dual-phase (DP) nor TRIP steels is new. The DP steels originated in 1975 [163] as a strip or sheet product and were the subject of intense research over the following next decade [164,165]. Carbon TRIP steels were first introduced as plate product in the late 1960's [166]. In these high carbon, highly alloyed steels, the TRIP reaction was used to attain very high strength properties, with yield strength levels exceeding 1400 MPa and total elongations of 30% [166].

Multiphase microstructures are currently used routinely in plate steels to reach beyond what is achievable with ferrite-pearlite steels. This is accomplished by water spray cooling the as-controlled rolled austenite at about 10°C/sec to the water end temperature, (WET), and then further air cooling to room temperature. Clearly, for a given CCT diagram, the choice of WET gives some flexibility to the final microstructural micro-constituents that can be obtained. An example of this phase balance is shown in Figure 34 [138]. In this work, Nb has played two important roles that are often found in this kind of microstructural development: (i) it has caused strong refinement of the final microstructure, which includes both the polygonal ferrite and the low temperature transformation products, i.e., bainite or martensite; and (ii) it has altered the nature of the final microstructure, often in the presence of interrupted accelerated cooling, through its effect as a solute on hardenability. Hence, the combination of the Nb and the interrupted accelerated cooling has enabled tensile strengths of 700 MPa to be achieved in 20 mm plate while maintaining very good toughness, Figure 35 [138].

Niobium has also proven to be instrumental in achieving excellent properties in both hot rolled strip and cold rolled and annealed sheet versions of multi-phase steels where strength, formability and sheared edge ductility are important. At the high strength levels involved, with tensile strengths around 700 MPa, the multiphase steels exhibit high levels of all of these properties [101,168].

In some early work on multiphase steels, the very important but perhaps underappreciated role of microstructural refinement on formability was presented, Figures 37 and 38 [169]. Figure 37 shows the expected relationship between the amount of retained austenite and work hardening rate in a so-called dual-phase steel containing a ferrite-martensite-retained austenite microstructure [169]. What is perhaps somewhat overlooked is the importance of the scale of the dispersion of the retained austenite, Figure 38. Clearly, a fine dispersion of retained austenite is advantageous in attaining higher rates of work hardening even at constant amounts of retained austenite. Since the interparticle spacing is directly related to the S_v of the hot rolled austenite, the importance of Nb in austenite conditioning during rolling is obvious.

Recent work on TRIP steels has shown a clear benefit of Nb to the microstructures, properties and manufacturability of these steels [102,169]. Again, the benefits of the Nb additions originate in its dual abilities to alter the transformation behavior of the hot rolled austenite and to cause microstructural refinement.

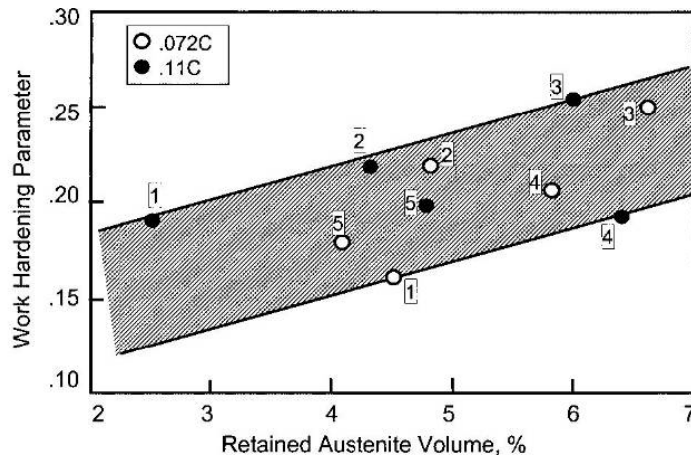


Figure 37. Variation in work hardening parameter with increasing retained austenite volume fraction [169].

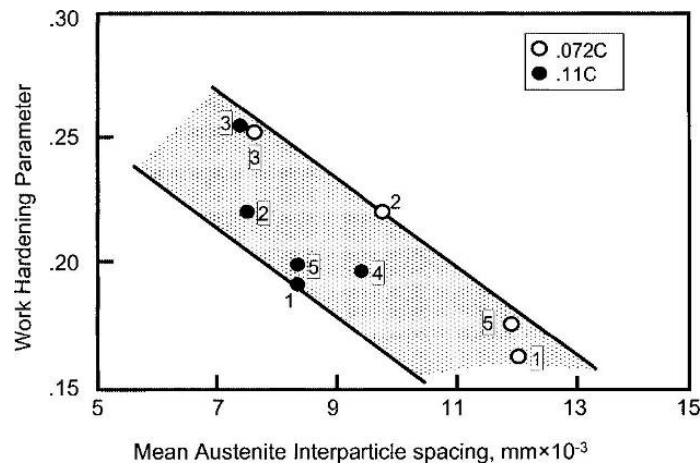


Figure 38. Correlation between work hardening parameter and mean austenite interparticle spacing [169].

The influence of microstructural refinement on work hardening rate (WHR) and total elongation can be traced back to early work of Ashby [170,171], in which he studied the work hardening of plastically heterogeneous materials. Ashby's work led to the equation:

$$\frac{d\sigma}{d\varepsilon} = \alpha G [(f b) / (D \varepsilon)]^{1/2} \quad (19)$$

where:

- α = constant near 1
- G = shear modulus
- b = Burgers vector
- f = volume fraction of hard phase
- D = diameter of hard phase.
- ε = strain

When this equation is expressed in terms of f and λ , the inter-island distance between hard volumes, the WHR varies as $\lambda^{-1/2}$. Hence, the work hardening rate is inversely related to the dispersion of the martensite-retained austenite islands in the DP steels and to the bainite-retained austenite islands in the TRIP steels; the finer the dispersion, the higher the work hardening rate. The experimental verification

of this theory has been clearly established for the martensite islands in DP steels [97,172]. Equation 31 explains, to some extent, the importance of Nb in these multiphase steels. The use of Nb allows very high values of S_v to be achieved for the controlled rolled austenite. Higher values of S_v mean smaller values of λ in equation 31, and, hence, higher values of both work hardening rates, and total elongations, and stretch formability.

In summary, Nb has long been recognized as being able to increase the strength of ferrite in ferrite – pearlite steels through various means. This has led to steels with yield strengths near 400 MPa. Higher strength steels have required multi-phase microstructures involving combinations of microconstituents such as ferrite and low temperature transformation products such as bainite and martensite. Research over the past two decades has shown that Nb is also important in achieving the proper microstructure and final properties in these newer steels. Besides its well recognized benefit to austenite conditioning, and, hence, to microstructural refinement, Nb has also been shown to play a critical role in helping control the evolution of final microstructure in these steels during plate, strip and sheet processing.

Niobium and Stabilization

Within the past ten years, niobium has become a popular addition to two important classes of steels, the ultra-low carbon (ULC) or interstitial-free (IF) steels and in ferritic stainless steels (FSS). The primary reason for making the addition of Nb was to complement Ti in the stabilization of carbon and nitrogen, i.e., the removal of C and N from solid solution, in these steels. However, later work has shown that the addition of Nb can have benefits far beyond simple stabilization. In ferritic stainless steels stabilization is used to remove the yield point and prevent strain aging, but it also plays the important role of reducing or eliminating sensitization. Sensitization is the intergranular corrosion caused by the precipitation of chrome carbides at the ferrite grain boundaries, thereby depleting the grain boundary region of sufficient chrome to prevent grain boundary attack [173,174]. In ULC steels, the stabilization is important mainly because it removes the yield point after either batch or continuous annealing, prevents strain aging, and it aids in the development of suitable crystallographic textures to enhance formability [175,176].

Niobium in IF Steels

The early IF steels were stabilized by Ti alone, where enough Ti was added to theoretically tie up all of the C, N and S in the steel [175]. The amount of Ti required for complete stabilization was often given as:

$$\text{Ti} = 4\text{C} + 3.42\text{N} + 1.5\text{S} \quad (20)$$

The first particle that forms with falling temperature is TiN. The subsequent behavior of Ti depends upon the initial sulfide that forms in the interdendritic pools [177]. For example, if the Mn is below about 2000 ppm, TiS is formed. TiS is a complex compound with a rhombohedral crystal structure that can exhibit numerous crystal structures or polytypes, based on the defect structure contained within the structure. It has been found that when both the bulk Ti content is high (over 0.06 wt%) and the Ti/S ratio is high (over 7), the 9-R rhombohedral form of TiS is formed. When the bulk Ti is lower (0.04), and the Ti/S ratio is lower (near 5), the 18-R and 6-R polytypes of TiS are formed. During subsequent cooling, the different polytypes of TiS behave differently. The 9-R polytype undergoes intercalation during cooling such that layers of Ti and C are added to the pre-existing layers of Ti and S to form the hexagonal or H- phase $\text{Ti}_4\text{C}_2\text{S}_2$ [177]. This results in the following in-situ transformation of TiS: [177]



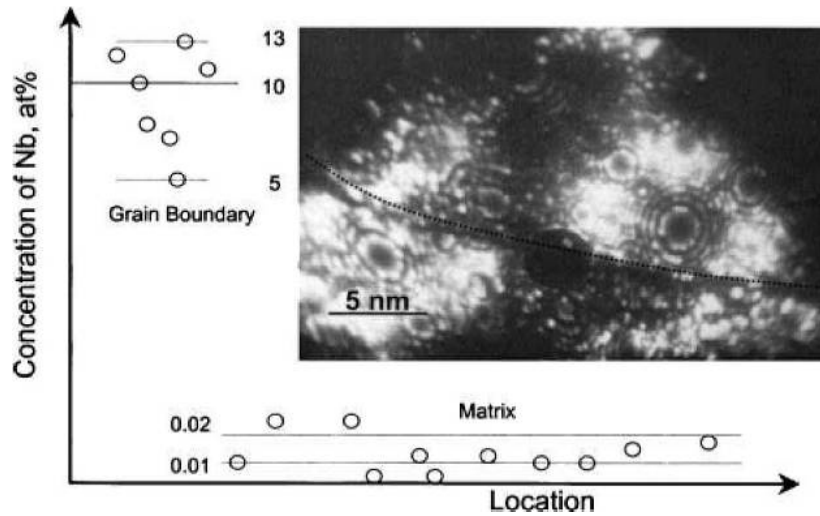


Figure 40. Concentrations of Nb on the grain boundary, on the subgrain boundary, and within the matrix, measured by APFIM from a finish rolled and/or coiled IF steel [177].

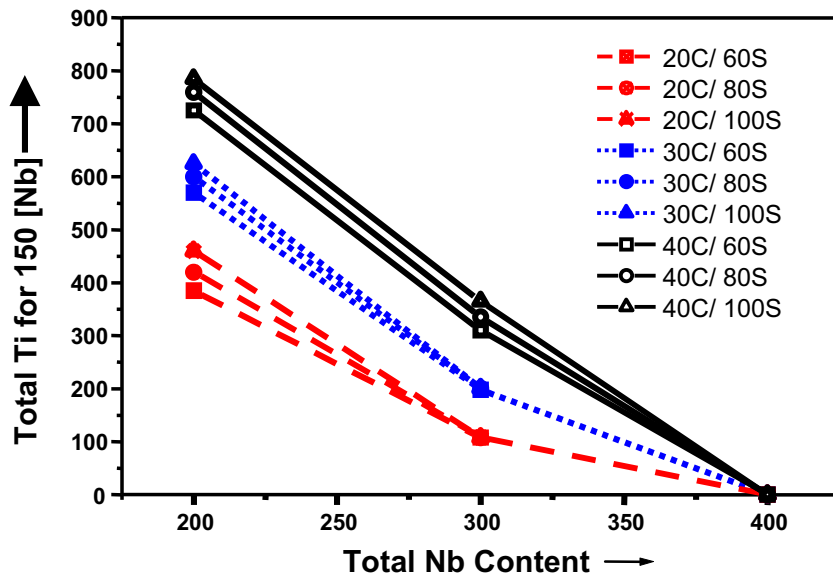


Figure 41. Alloy design for keeping 150 ppm Nb in solution [183].

If solute Nb on the ferrite grain boundaries is the key to better resistance to the outburst phenomenon, and if solute Nb at the free surface is the key to better coating adherence, two questions arise: (i) how much solute Nb is needed for significant improvement? and (ii) how does one get this solute level? Recent work has shown that the galvannealing performance of a dual stabilized IF steel was much better than that for a Ti stabilized IF steel [182]. In this work, about 150 ppm Nb was estimated to be in solution at room temperature. The following diagram, Figure 41, illustrates the combinations of additions of Ti and Nb for given levels of C and S that would be needed in a typical IF steel in order to guarantee that 150 ppm Nb would remain in solution at room temperature [183]. This figure shows, for example, that for IF steels containing 30 ppm C, 30 ppm N, 80 ppm S and 600 ppm Ti, a Nb addition of 200 ppm would be required for a Nb solute level of 150 ppm. A similar steel containing 40 ppm C would require a bulk Nb content of about 240 ppm to keep the 150 ppm Nb in solution. A research program is currently in progress to better define the compositional requirements of the steel substrate for superior galvannealing.

Finally, there are two other important effects that have been attributed to solute Nb that has segregated to the ferrite grain boundaries. First, it has been shown to be important in helping overcome the deleterious effects of P in cold or secondary work embrittlement [179,184,185]. Second, it has been shown to be important in improving the crystallographic texture in cold rolled and annealed IF steels [179,186-188].

Niobium in Ferritic Stainless Steels

In 1997, the North American stainless steel industry produced approximately 2.4 million tons of steel of which about 62% was austenitic stainless and 33% was ferritic stainless. Of the austenitic stainless steels produced, T304 and derivatives were the largest group representing about 62%, with T316 representing 13% and T301 representing about 10%. On the ferritic stainless side, T409 represented about 67% of the total ferritics, with T43X representing about 12% and T439 representing about 4.2%. Within the last decade, the growth in use of Nb in ferritic stainless steels in North America was extremely strong. This has been particularly true in T409 used mainly for automotive exhaust systems.

In general, Nb is added to ferritic stainless steels to achieve several benefits that include:

- Intergranular corrosion resistance (stabilization)
- Creep resistance
- Roping and ridging resistance
- Oxidation resistance
- Improved surface quality
- Improved die wear during forming

These advantages have been discussed and explained elsewhere [189,190].

The first stabilized ferritic stainless steel intended for the automotive exhaust system was developed by Allegheny Ludlum in 1961. This steel contained 12% Cr, was fully stabilized with Ti, and now has the designation UNS S40900. Over the past decade, dual stabilization of T409 with Ti + Nb has become a popular alternative to the earlier Ti-only approach. The dual-stabilized T409 steels fall under the classification of UNS S40930. There are several reasons for this change in stabilization systems; these have been reviewed by Franson and Fritz [191].

The effectiveness of Ti + Nb as a stabilization system is shown in Figure 42 [191]. Figure 42 indicates that while the choice of Ti alone or in combination with Nb would appear to be equivalent, this choice has ramifications far beyond simple sensitization and stabilization. For example, T409 stabilized with the combination of Ti + Nb, designated as T466, shows an improvement in creep or sag resistance, especially between 600°C and 800°C, Figure 43 [191]. Also, the oxidation resistance of dual-stabilized T466 is much better than that of the Ti-only T409, Figure 44 [191]. The benefits of the Nb additions shown in Figures 43 and 44 are probably caused by a combination of solute and precipitated Nb. As noted earlier, other benefits of Nb additions in dual-stabilized T409 include improvements in texture formation and formability [192,193], surface quality, and die wear [189-193].

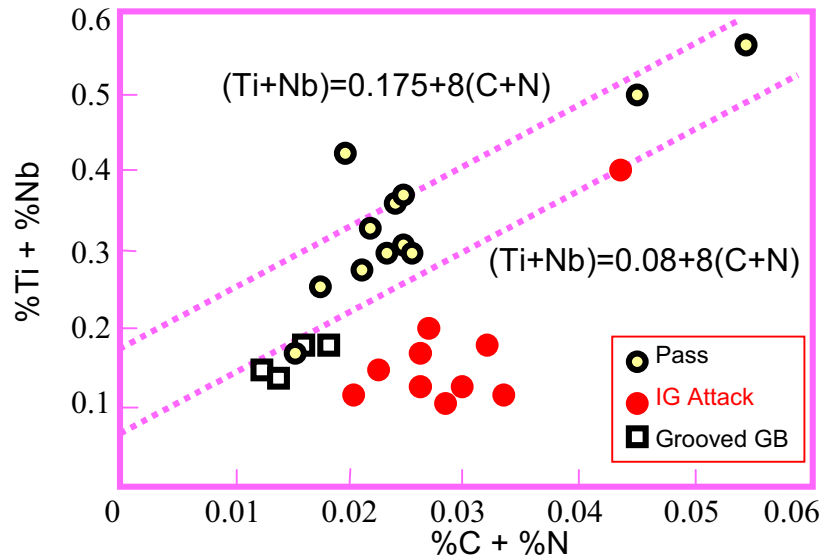


Figure 42. Resistance to intergranular corrosion in the heat affected zone as a function of stabilization [191].

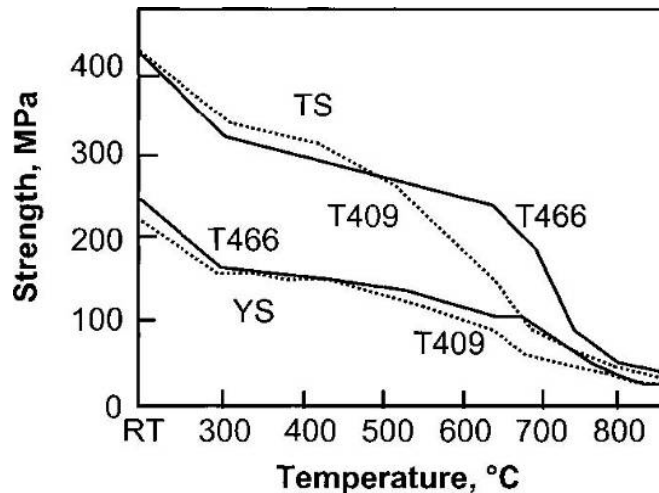


Figure 43. Elevated temperature tensile properties [189,190].

To explain some of these differences in behavior, a study is currently being conducted of the precipitation in single stabilized (Ti) and dual-stabilized (Ti+Nb) T409 ferritic stainless steel. Preliminary results indicate that there are clear differences in the precipitation behavior [194]. Both steels showed precipitation of TiN that had occurred at high temperature, possibly in the liquid or in the interdendritic pools, that was stable during subsequent processing. In the Ti-only steel, precipitation of TiC upon cooling occurred between 830°C and 780°C. The TiC was observed on the pre-existing TiN, on the ferrite grain boundaries and in the matrix. The precipitation sequence in the dual-stabilized steel was similar. There were two major differences in precipitation between the two steels. First, the carbide in the dual-stabilized steel was a mixed (TiNb)C. Second, the precipitation in the dual-stabilized steel occurs at much higher temperatures upon cooling than in the Ti-only steel, i.e., near 1200°C as compared to the 830 - 780°C range for the Ti-only T409. An example of the epitaxial precipitation of (TiNb)C on TiN in the dual-stabilized T409 is shown in Figure 45 [194]. This difference in precipitation temperature can have important ramifications regarding the behavior during hot deformation. The fact that the C in the dual-stabilized T409 is stabilized at temperatures near 1200°C

means that most, if not all, of the hot rolling of ferrite in this steel in a typical strip mill will occur in the absence of solute carbon. This will not be the case for the Ti-only steel since the TiC does not form until 830°C, or while the strip is on the runout table or in the coil. The absence of solute carbon during hot rolling of the ferrite in the dual-stabilized T409 is expected to aid in the formation of beneficial texture components. The effect of solute carbon on texture development has been observed repeatedly in the ULC steels discussed above [175,176,179,187,188,195].

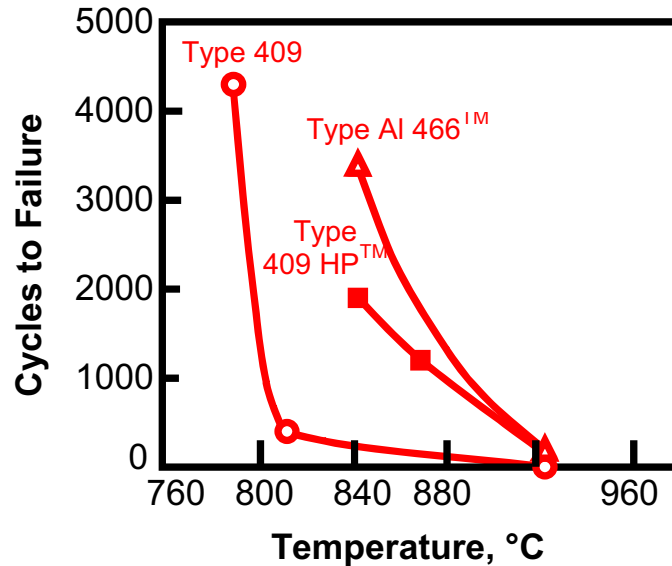


Figure 44. The still air cyclic oxidation resistance of Type 409, Type 409 HP™ (low interstitial) and Type 466™ (low interstitial, dual-stabilized) steels [189,190].

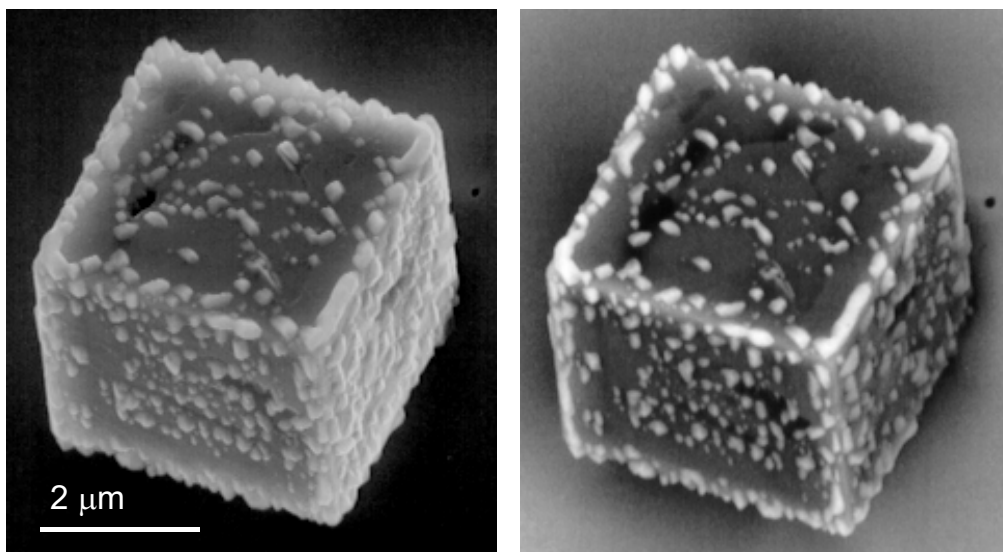


Figure 45. Secondary electron micrograph and back scattering image of a large cube-shaped (TiNb)(CN) particle, with small epitaxial NbC particles attached [194].

Summary

The past twenty years have witnessed growth in both the applications of Nb in steels and in our understanding of how Nb affects its benefits. Furthermore, niobium additions are now the basis for new high strength multi-phase steels for both strip and plate applications. Other new applications include stabilization of both IF steels and ferritic stainless steels. Perhaps the most important new finding concerning the behavior of Nb is the role played by solute Nb in improving a wide range of structure, properties and performance. Since the first commercial Nb steel was produced in 1958, the impressive benefits attainable through the addition of this microalloying element has spawned nearly five decades of intense research. Some of this work was aimed at simply documenting the benefits of improved microstructure, properties or processing. Others chose to delve into the mysteries of how Nb acted to create its powerful effect. The story of the use of Nb in steel is by no means complete nor concluded here in 2001, to which the researchers 20 years hence will surely attest.

References

1. Charles Hatchett, as cited in Palache et al., ref. 2.
2. C. Palache, H. Berman and C. Frondel, *The System of Mineralogy*, (ed. J.D. Dana and E.S. Dana), 7th Edition, vol. 1, (New York, NY: J. Wiley & Sons, 1944), 1082.
3. O. De Souza Paraiso Filho and R. De Fuccio, Jr., *Niobium*, (ed. H. Stuart), (Warrendale, PA: The Metallurgical Society of AIME, 1984), 113-132.
4. F.M. Becket and R. Franks, U.S. Patent 2158651, May 16, 1939.
5. C.A. Beiser, "The Effect of Small Columbium Additives to Semi-Killed Medium Carbon Steels", (Metals Park, OH: American Society for Metals, 1959), ASM preprint no. 138.
6. H. Stuart, ed., *Fundamental Metallurgy of Niobium in Steel*, "Niobium '81", (Warrendale, PA: The Metallurgical Society of AIME, 1984).
7. A. J. DeArdo, J. M. Gray and L. Meyer, in Proc.of Int. Symposium "Niobium '81", (ed., Harry Stuart), (Warrendale, PA: The Metallurgical Society of AIME, 1984), 685-759.
8. A. J. DeArdo, "Niobium in Modern Steels," *International Materials Reviews*, 48 (6) (2003), 371-402.
9. H. Watanabe, Y.E. Smith and R.D. Pehlke, *The Hot Deformation of Austenite*, (ed. John B. Balance), (New York, NY: TMS-AIME, 1977), 140-168.
10. T. Mori, K. Fujita, M. Tokizane and K. Yamaguchi, *Tetsu-to-Hagane, J. Iron Steel Inst. Jpn.*, 50 (1964), 911-917.
11. W.A. Bandi, private communication with author, United States Steel Corporation Research Laboratories 1979.
12. L. Meyer, H.E. Bühler and F. Heisterkamp, *Thyssenforschung*, 3 (1971), 8-43.
13. M.L. Santella, "Grain Growth and High-Temperature Hot Rolling Behavior of Low-Alloy Steel Austenite", Ph.D. Thesis, University of Pittsburgh, (1981), 49.
14. C. J. Smithells, *Metals Reference Book*, 4th Edition, (London, UK: Butterworths, 1967), 155.
15. W.B. Pearson, *Handbook of Lattice Spacings and Structures of Metals and Alloys*, Vol. 2, (London, UK: Pergamon Press, 1958), 124.
16. P. Duwez and F. Odell, *J. Electrochem. Soc.*, 97 (1950), 299-304.
17. G. Bauer, H. Renner and J. Wernet, *Z. Anorg. Allg. Chem.*, 277 (1954), 249-257.
18. E.K. Storms and N.H. Krikorian, *J. Phys. Chem.*, 64 (1960), 1471.
19. J.M Gray, *Heat Treatment*, (London, UK: The Metals Society, 1973), 19-28.
20. G. Brauer and J. Jander, *Z. Anorg. Allg. Chem.*, 270 (1952), 160-178.
21. R.P. Elliott, *Trans. Am. Soc. Metals*, 53 (1961), 13-28.
22. S. Kanazawa, A. Nakashima, K. Okamoto and K. Tanabe and S. Nakazawa, *Nippon Kinzoku*

- Gakkaishi*, 31 (2) (1967), 171-176.
23. G. Krapf, E.G. Buyok, E.G. Bandiand L.M. Melnick, *J. Iron Steel Inst.*, 211 (1973), 353-356.
 24. H. Nordberg and B. Aronson, *J. Iron Steel Inst.*, 206 (1968), 1263-1266.
 25. P. Mandry and W. Dornelas, *C.R. Acad. Bulg. Sci.*, 263 (1966), 1118-1121.
 26. C. Ouchi and H. Iizumi, *Effects of Interstitial and Substitutional Solute Elements on the Recrystallization Temperature of High Purity Steels*, (ed. T. Sakai *et al.*), (Tokyo, Japan: The Japan Institute of Metals, 1999), 79-88.
 27. R. Grimaldi, S. Maneschi and N. Vantini, *Arch. Eisenhüttenwes*, 38 (5) (1967), 401-406.
 28. T. Mori, M. Tokizane and K. Okamoto, *Tetsu-to-Hagane*, 51 (1965), 2034-2036.
 29. S. Maneschi and A.M. Beccaria, *Metall. Ital.*, 58 (1) (1966), 19-24.
 30. Hoesch-Estel, Dortmund, Germany, Unpublished results.
 31. W.A. Roberts, A. Sandberg and T. Siwecki, *Vanadium Steels* (Krakow), (London, UK: Vanitec, 1981), 19.
 32. E.L. Brown, A.J. DeArdo and J.H. Bucher, *The Hot Deformation of Austenite*, (ed. John B. Balance), (New York NY: TMS-AIME, 1977), 250-285.
 33. P. Schwaab and G. Langenscheid, *Prakt. Metallogr.*, 9 (2) (1972), 67-75.
 34. R.E. Reed-Hill, *Physical Metallurgy Principles*, 2nd Edition, (New York, NY: Van Nostrand), 73.
 35. R.E. Reed-Hill, *ibid*, 480.
 36. E.J. Palmiere, *Suppression of Recrystallization during the Hot Deformation of Microalloyed Austenite*, PhD Thesis, University of Pittsburgh, (1991).
 37. C.H.P. Lupis, *Chemical Thermodynamics of Materials*, (New York, NY: Elsevier Science Publishing Co., 1983), 345.
 38. D.R Gaskell, *Introduction to Metallurgical Thermodynamics*, 2nd Edition, (New York, NY: McGraw Publishing Co., 1981), 419.
 39. C. Wagner, *Thermodynamics of Alloys*, (Massachusetts: Addison-Wesley, 1952), 47.
 40. J. Chipman, *J. Iron Steel Inst.*, 180 (6) (1955), 97.
 41. D.A. Porter and K.E. Easterling, *Phase Transformations in Metals and Alloys*, (Reinhold, UK: Van Nostrand, 1981), 44.
 42. C.H.P. Lupis, *Chemical Thermodynamics of Materials*, (New York, NY: Elsevier Science Publishing Co., 1983), 363.
 43. R.P. Smith, *T. Metall. Soc. AIME*, 236 (2) (1966), 220.
 44. T.H. Johansen, N. Christensen and B. Augland, *T. Metall. Soc. AIME*, 239 (10) (1967), 1651.
 45. T. Mori, M. Tokizane, K. Yamaguchi, E. Sunami, and Y. Nakazima, *Tetsu-to-Hagane*, 54 (1968), 763-776.
 46. H.L. Andrade, M.G. Akben, and J.J. Jonas, *Metall. Trans.*, 14A (10) (1983), 1967-1977.
 47. R.C. Sharma, V.K. Lakshmanan and J.S. Kirkaldy, *Metall. Trans.*, 15A (3) (1984), 545.
 48. V.K. Lakshmanan and J.S. Kirkaldy, *Metall. Trans.*, 15A (3) (1984), 541-544.
 49. K. Balasubramanian and J.S. Kirkaldy, *Advances in Phase Transitions*, (ed. J.D. Embury *et al.*), (Oxford, UK: Pergamon Press, 1988), 37.
 50. K. Narita, *T. Iron Steel I. Jpn.*, 15 (3) (1975), 145.
 51. R.P. Smith, *T. Metall. Soc. AIME*, 224 (1962), 190.
 52. K.J. Irvine, F.B. Pickering and T. Gladman, *J. Iron Steel Inst.*, 205 (1967), 161-182.
 53. T.M. Hoogendoorn and M.J. Spanraft, *Microalloying '75*, (New York, NY: Union Carbide Corporation, 1977), 75-85.
 54. R.C. Hudd, A. Jones and M.N. Kale, *J. Iron Steel Inst.*, 209 (2) (Feb. 1971), 121.
 55. S. Koyama, T. Ishii and K. Narita, *J. Jap. Inst. Materials*, 35 (11) (1979), 1089-1094.

56. R.A. Swalin, *Thermodynamics of Solids*, 2nd Edition, (New York, NY: John Wiley and Sons, 1972), 165.
57. R. Simoneau, G. Begin and A.H. Marquis, *Met. Sci.*, 12 (8) (1978), 381.
58. T. Gladman, D. Dullieu and I.D. McIvor, *Microalloying '75*, (New York, NY: Union Carbide Corporation, 1977), 35-58.
59. E. Listhuber, *High Strength Micro-Alloyed Steels Symposium*, (Dusseldorf, Germany: Metallurg Companies, 1970), 29-34.
60. J. Wadsworth, S.R. Keown, and J.H. Woodhead, *Met. Sci.*, 10 (3) (1976), 105-112.
61. S.R. Keown and W.G. Wilson, *Thermomechanical Processing of Microalloyed Austenite*, (ed., A.J. DeArdo *et al*), (Pittsburgh, PA: TMS-AIME, 1981), 343-359.
62. C.H.P. Lupis, *Chemical Thermodynamics of Materials*, (New York, NY: Elsevier Science Publishing Co., 1983), 523.
63. E.J. Palmiere, C.I. Garcia, and A.J. DeArdo, *Metall. Mater. Trans. A*, 25A (1994), 277.
64. E.J. Palmiere, C.I. Garcia and A.J. DeArdo, *Metall. Mater. Trans. A*, 27A (4) (1996), 951.
65. J.F. Elliott, *Electric Furnace Steelmaking: Theory and Fundamentals*, Vol. II, (New York, NY: Interscience, 1963), 95-178.
66. W.C. Leslie, *The Physical Metallurgy of Steels*, (New York, NY: Hemisphere Publishing, 1981), 68.
67. H. Takechi, *ISIJ Int.*, 34 (1) (1994), 1-8.
68. O. Hashimoto, S. Satoh, T. Irie and N. Ohashi, *Proc. Int. Conf. on Advances in Physical Metallurgy and Applications of Steel*, (London, England: The Metals Society, 1984), 95-104.
69. K.A. Taylor, *Scripta Metall.*, 32 (1) (1995), 7-12.
70. T. Gladman, *The Physical Metallurgy of Microalloyed Steels*, (London, UK: Institute of Materials), 1997.
71. D.H. Jack and K.H. Jack, *Mater. Sci. Eng.*, 11 (1) (1973), 1-27.
72. A.T. Davenport and R.W.K. Honeycombe, *Met. Sci.*, 9 (5) (1975), 201-208.
73. R.W.K. Honeycombe, *Metall. Mater. Trans. A*, 7A (1976), 915-936.
74. J. M. Silcock, *J. Iron Steel Inst.*, 201 (1963), 409-421.
75. J.S.T. Van Aswegen, R.W.K. Honeycombe and D.H. Warrington, *Acta Metall.*, 12 (1) (1964), 1-13.
76. J. M. Silcock, *Acta Metall.*, 14 (5) (1966), 687-692.
77. F. H. Froes, R.W. Honeycombe and D.H. Warrington, *Acta Metall.*, 15 (1967), 157-159.
78. M. Tanino and K. Aoki, *T. Iron Steel I. Jpn.*, 8 (5) (1968), 337-345.
79. R.G. Baker and J. Nutting, *Precipitation Processes in Steels*, Iron and Steel Institute Special Report No. 64, (London, 1959), 1.
80. G. Kurdjumov and G. Sachs, *Z. Phys.*, 62 (1930), 592.
81. S. Kurokawa, J.E. Ruzzante, AM. Hey and F. Dymont, *Niobium Diffusion in Iron and Some Iron Base Alloys*, XXXVI Congresso Annual de ABM, 36 (1) (San Paulo, Brasil: Brazilian Association of Metals, 1981) 47-63.
82. P.L. Mangonon and W. E. Heitmann, in Proc. Conf. 'Microalloying '75, 1977, New York, Union Carbide Corporation, 59-70.
83. G. Gauthier and A.B. Le Bon, in Proc. Conf. 'Microalloying '75', 1977, New York, Union Carbide Corporation, 71-74.
84. A.T. Davenport, R. E. Miner and R. A. Kot, 'The Hot Deformation of Austenite', ed. John B. Balance, 186-203; 1976, New York, TMS-AIME.
85. J. Irvine and T.N. Baker, *Met. Sci.*, 1979, 13, 228-237.
86. S.S. Hansen, J.B. Vander Sande and M. Cohen, *Metall. Mater. Trans. A*, 1980, 11, 387-402.
87. A. T. Davenport, L. C. Brossard and R. E. Miner, *JOM*, 1975, 27, 21-27
88. J.M. Gray and R.B.G. Yeo, *ASM Trans. Q.*, 1968, 61(2), 255-269.

89. A. Mascanzoni and G. Bussichelli, *Philos. Mag.*, 1974, 30(1), 207-212.
90. S. Freeman, 'Effect of Second Phase Particles on the Mechanical Properties of Steel', ISI Special Publication No. 145, London, 1971, 152.
91. G.R. Speich, L.J. Cuddy, C.R. Gordon and A.J. DeArdo, in 'Phase Transformations in Ferrous Alloys', (ed. A.R. Marder *et al*), 341-390; 1984, Warrendale, TMS-AIME.
92. A.J. DeArdo, 'HSLA Steels', 70-79; 1985, Port Kembla, South Coast Printers.
93. A. J. DeArdo, in Proc. Conf. 'Thermec '97', (eds. T. Chandra and T. Sakai), Dec. 1977, Vol. 1, TMS Publications, 13-30.
94. A. D. Wilson, E. G. Hamburgh, D. J. Colvin, S. W. Thompson and G. Krauss, "Properties and Microstructures of Copper Precipitation Aged Plate Steels," *Microalloyed HSLA Steels*, (Materials Park, OH: ASM International, 1988), 259-276.
95. J. M. Rigsbee and P.J. VanderArend, in 'Formable HSLA and Dual-Phase Steels', Vol. 244, (ed. A.T. Davenport), 56-86; 1979, New York, Metallurgical Society of AIME .
96. F. B. Pickering, 'HSLA Steels: Technology and Applications', 1-31; 1984, Ohio, ASM.
97. C.A.N. Lanzillotto and F.B. Pickering, *Metall. Sci.*, 1982, 16, 371-382.
98. N.K. Balliger, 'Advances in the Physical Metallurgy and Applications of Steels', 73; 1983, London, The Metals Society.
99. J.T. Barnby, *Acta Mater.*, 1967, (5), 903-909.
100. E. Smith, *Int. J. of Fract.*, 1968, 4, 131.
101. K. Hulka, W. Bleck and K. Papamantellos, in Proc. Conf. '41st MWSPC', Baltimore, MD., Oct. 1999, AIME, 67-78.
102. T.Heller, B. Engl, G. Thiemann and G. Stich, in Proc. Conf. 'Thermomechanical Rolling of Hot Rolled Multiphase Steels', London, England, 2000, IOM Communications Ltd., 438-445.
103. A.J. DeArdo, in Proc. Conf. 'Microalloying in Steels: New Trends for the 21st Century', San Sebastian, Sept., 1998, (ed., J. M. Rodriguez-Ibabe, I. Gutiérrez and B. López), 15-26.
104. A. LeBon, *Met. Sci*, 1975, 9, 36-40.
105. R. Coladas, J. Masounave and J.P. Bailon, in 'The Hot Deformation of Austenite', (ed. John B. Balance), 341-378; 1977, New York, TMS-AIME.
106. J.J. Jonas and I. Weiss, *Met. Sci.*, 1979, 13, 238-245.
107. D. Webster and J. H. Woodhead, *J. Iron Steel Inst.*, 1964, 202, 987-994.
108. J.D. Jones and A.B. Rothwell, 'Deformation Under Hot Working Conditions', ISI Publication No. 108, 78-82, 1968, London, The Iron and Steel Institute.
109. J.M. Gray, 'Processing and Properties of Low Carbon Steel', (ed. J.M. Gray), 225-247; 1973, New York, The Metallurgical Society of AIME.
110. L. Meyer, F. Heisterkamp and W. Mueschenborn, in Proc. Conf. 'Microalloying '75', Washington, DC, Oct. 1975, (ed. M. Korchynsky *et al.*), Union Carbide Corporation, 153-167.
111. R. Simoneau, G. Begin and A.H. Marquis, *Met. Sci.*, 1978, 12(8), 381-386.
112. G. Begin and R. Simoneau, in Proc. Conf. 'Microalloying '75, New York, 1977, Union Carbide Corporation, 85-87.
113. C. Ouchi, T. Sanpei, T. Okita and I. Kozasu, in 'The Hot Deformation of Austenite', (ed. John B. Balance), 316-340; 1977, New York, AIME.
114. R.K. Amin, G. Butterworth and F.B. Pickering, in 'Hot Working and Forming Processes', 27-31; 1979, London, The Metals Society.
115. M.G. Akben, I. Weiss, and J.J. Jonas, *Acta Metall. Mater*, 1981, 29, 111-121.
116. A.J. DeArdo, *Ironmaking and Steelmaking*, 2001, 28, (2), 138-144.
117. M.E. Fine, 'Phase Transformations in Condensed Systems', 1964, New York, McMillan Publishing.

118. D.J. Swinden, and J.H. Woodhead, *J. Iron Steel Instit.*, 1971, 209, 883-899.
119. I. Kozasu, C. Ouchi, T. Sampei and T. Okita, in Proc. Conf. 'Microalloying '75', New York, 1977, Union Carbide Corporation, vol. 1, 120-135.
120. J. D. Grozier, in Proc. Conf. 'Microalloying '75', New York, 1976 (ed. M. Korchynsky), Union Carbide Corporation, 241-250.
121. K. Amano, T. Hatomura, M. Koda, C. Shiga and T. Tanaka, in Conf. Proc. 'Accelerated Cooling of Steel', (ed. P.D. Southwick), Warrendale, PA, 1986, The Metallurgical Society, 349-365.
122. A. J. DeArdo, Influence of Thermomechanical Processing and Accelerated Cooling on Ferrite Grain Refinement in Microalloyed Steels, (Warrendale, PA: TMS-AIME, 1986), 97.
123. T. Tanaka, 'Overview of Accelerated Cooled Steel Plate', 187-208; 1988, New York, Pergamon Press.
124. A. J. DeArdo, *Can Metall. Q.*, 1988, 27, 141.
125. E.E. Underwood, in 'Quantitative Microscopy', (eds. R.T. DeHoff and F.N. Rhines), 77-127; 1968, New York, McGraw-Hill Book Company.
126. L.J. Cuddy, *Metall. Trans*, 1984, 15A, 87-98.
127. H. Sekine and T. Maruyama, *Seitetsu Kenkyu*, 1976, 289, 43-61.
128. H. Sekine, T. Maruyama, H. Kageyama and Y. Kawashima, in Proc. Of International Conf. 'Thermomechanical Processing of Microalloyed Austenite', Pittsburgh, PA., August 1981 TMS-AIME, 141.
129. E.J. Palmiere, University of Pittsburgh, Unpublished Research, 1990.
130. O. Kwon and A. J. DeArdo, *Acta Metall Mater.*, 1991, 39, 529.
131. G.A. Wilber, J.R. Bell, J.H. Bucher and W.J. Childs, *Trans. Metall. Soc.*, 1968, 242(11), 2305-2308.
132. J.N. Cordea, in Proc. Conf. 'Symposium on Low Alloy High Strength Steels', Nürnberg BRD, May 1970, Metallurgical Companies, 61-80.
133. A. J. DeArdo, Unpublished Research, 1985.
134. S. Yamamoto, C. Ouchi and T. Osuka, 'The Effect of Microalloying Elements on the Recovery and Recrystallization in Deformed Austenite', (ed. A.J. DeArdo, *et al*), 613-638; 1982, Pittsburgh, PA, The Metallurgical Society of AIME.
135. L.J. Cuddy, in 'Thermomechanical Processing of Microalloyed Austenite', (ed. A.J. DeArdo *et al*), 129-140; 1982, New York, TMS-AIME.
136. L. Meyer, Thyssen Aktiengesellschaft, Duisburg-liamborn, 1981, Private Communication.
137. J.M. Gray, 'Weldability of Niobium-Containing High-Strength Low Alloy Steel', Bulletin No. 213, Welding Research Council, February 1976.
138. S. Okaguchi, T. Hashimoto and H. Ohtani, in Proc. Conf. 'Thermec '88', Tokyo, Japan, 1988, Iron and Steel Institute of Japan, vol. 1, 330-336.
139. H. Tamehiro, R. Habu, N. Yamada, H. Matsuda and M. Nagumo, in 'Accelerated Cooling of Steel', (ed. P.D. Southwick), 401-413; 1986 Warrendale, PA, The Metallurgical Society.
140. K. Abe, M. Shimizu, S. Takashima and H. Kaji, in Proc. Conf. 'Thermec '88', Tokyo, Japan, June 1988, The Iron and Steel Institute of Japan, Vol. 1, 322-329.
141. W.M. Hof, M.K. Gräf, H.-G. Hillenbrand, B. Hoh and P.A. Peters, in 'HSLA Steels: Metallurgy and Applications', (ed. J.M. Gray *et al.*) 467-474, 1986, Metals Park, OH, ASM International.
142. P. Bufalini, N. Pontremoli, A DeVito and A. Aprile, in 'HSLA Steels: Technology and Applications', 743-754; 1984, Metals Park, OH: ASM International.
143. M.K. Graf, P.A. Peters, F.K. Lorenz, P. Schwaab, 'HSLA Steels: Technology and Applications', 801-807; 1984, Metals Park, OH: ASM International.
144. R.L. Bodnar and S.S. Hansen, in Proc. Conf. '38th Mechanical Working and Steel

- Processing', Warrendale, PA, 1997, Iron and Steel Society of AIME, Vol. XXXIV, 513-525.
145. V. Thillou, M. Hua, C.I. Garcia, C. Perdrix and A.J. DeArdo, 'Microalloying in Steels' (ed. J.M. Rodriguez-Ibabe *et al.*), 311-318; 1998, Switzerland, Trans Tech Publications.
 146. V. Thillou, M. Hua, C.I. Garcia, C. Perdrix and A.J. DeArdo, in Proc. Conf. '41st Mechanical Working and Steel Processing Conference' Baltimore, MD., Oct. 1999, The Iron and Steel Society of AIME, 471-482.
 147. A.J. DeArdo, Reducing the Variability of HSLA Sheet Steels, American Iron and Steel Institute/Department of Energy Technical Roadmap Program, Project No. 9807, Sixth Quarterly Report, December 31, 2000.
 148. F.Y. Sun, W. Xu and X Ma, in 'HSLA Steels: Metallurgy and Applications', 277-286; 1985, Metals Park, OH, ASM International.
 149. T.N. Baker, 'Yield, Flow and Fracture of Polycrystals', (ed. T.N. Baker), 235-273; 1983, Applied Science Publishers.
 150. E. Hornbogen, 'Strength of Metals and Alloys', (ed. P. Haasen *et al.*), 1337-1342; 1979, Vol. 2,
 151. J. Irvine and T.N. Baker, *Mater. Sci. Eng.*, 1984, 64, 123-134.
 152. H. Kejian and T.N. Baker, *Mater. Sci. Eng.*, 1993, A169, 53-65.
 153. M. Hua, C. I. Garcia and A. J. DeArdo, University of Pittsburgh, 1996, Unpublished Research.
 154. R.W.K Honeycombe, 'Phase Transformations in Ferrous Alloys', (ed. A.R. Marder *et al.*), 259-280; 1988, Warrendale, PA, TMS-AIME.
 155. R.W.K. Honeycombe, in 'Processing Microstructure and Properties of HSLA Steels' (ed. A.J. DeArdo), 1-14; 1988, Warrendale, PA, TMS-AIME.
 156. T. Sakuma and R.W.K Honeycombe, *Met. Sci.*, 1984, 18, 449-454.
 157. T. Sakuma and R.W.K. Honeycombe, *Mater. Sci. Technol.*, 1985, 1, 351-356.
 158. T. Parayil and G. Ludkovsky, "Accelerated Cooling of Rolled Steel", (ed. G. E. Ruddle *et al.*), 131-146; 1988, New York, Pergamon.
 159. M. Hua, University of Pittsburgh, Unpublished Research, 2000.
 160. H. Gondoh and T. Osuka, 'Niobium', (ed. H. Stuart), 833-882; 1984, Warrendale, PA, TMS.
 161. T. Gladman, in Proc. Conf. 'Microalloying '75', New York, NY. 1977, Union Carbide Corporation, 32-54.
 162. J.M. Gray, in 'Heat Treatment '73', 19-28; 1973, London, The Metals Society.
 163. S. Hayami and T. Furukawa, in Proc. Conf. 'Microalloying '75', New York, NY, 1977, Union Carbide Corporation, 311-321.
 164. R.A. Kot and B.L. Bramfitt, In Proc. Conf. 'Fundamentals of Dual-Phase Steels: Proceedings of a Symposium', Warrendale, PA, 1981, The Metallurgical Society of AIME).
 165. A.T. Davenport, In Proc. Conf. 'Formable HSLA and Dual-Phase Steels: Proceedings of a Symposium', New York, NY, 1979, The Metallurgical Society of AIME, 244.
 166. V.F. Zackay, E.R. Parker, D. Fahr and R. Busch, *T. Am. Soc. Metal*, 1967, 60, 252-259.
 167. Z. Hanzaki, P. Hodgson and S. Yue, *Metall. Trans.*, 1997, 28A, 2405-2414.
 168. B. C. De Cooman, ed., Proc. Conf. on TRIP-aided High Strength Ferrous Alloys, 2002, Aachen, Wissenschaftsverlag Mainz.
 169. J.M. Rigsbee and P.J. Vander Arend, 'Formable HSLA and Dual-Phase HSLA Steels', (ed. A. T. Davenport), 56-86; 1979, New York, AIME.
 170. M.F. Ashby, *Philos. Mag.*, 1970, 8(21), 399-424.
 171. K.C. Russell, *Acta Met.*, (1970), 18, 891-901.
 172. N.K. Ballinger and T. Gladman, *Met. Sci.*, 1981, 15, 95-108.
 173. R.P. Frankenthal and H.W. Pickering, *Journal of Electrochemical Society*, 1973, 120 (1), 23-26.

174. W.C. Leslie, 'The Physical Metallurgy of Steels', 343; 1981, New York, NY, Hemisphere Publishing.
175. I. Gupta and D. Bhattacharya, in 'Metallurgy of Vacuum-Degassed Steel Products', (ed. R. Pradhan), 43-72; 1990, Warrendale, PA, AIME.
176. A.J. DeArdo, in Proc. Conf. 'IF Steels 2000', Warrendale, PA, 2000, ISS-AIME, 125-136.
177. M. Hua, C.I. Garcia and A.J. DeArdo, *Metall. Trans. A*, 1997, 28A, 1769-1780.
178. M.J. Hua, C.I. Garcia and A.J. DeArdo, Proc. Conf. for Inter. Symposium on "Modern L.C. and ULC Sheet Steels for Cold Forming, Processing and Properties", Wissenschaftsverlag, Aachen, Germany, March 30-Apr 1, 1998, (ed. W. Bleck and Verlag Mainz) Institute of Ferrous Metallurgy, 145-156.
179. G. Tither, C.I. Garcia, M. Hua and A.J. DeArdo, "Precipitation Behavior and Solute Effect in Interstitial-Free Steels," in Physical Metallurgy of IF Steel, *ISIJ*, Tokyo, 1994, 293-322.
180. M.F. Shi, G. M. Smith, M. Moore, and D. J. Meuleman, "Zinc Based Coatings Systems: Metallurgy and Performance," (Conf. Proc.), 387-398; 1990, Warrendale, PA, TMS-AIME.
181. G. Jenkins, Welsh Technology Centre, Corus Group, 1999, Unpublished Research.
182. C.C. Cheng, in Proc. Conf. '42nd MWSP', 2000, ISS, 255-263.
183. A.J. DeArdo, University of Pittsburgh, 1999, unpublished research.
184. N. Kino, M. Yamada, Y. Tokunaga and H. Tsuchiya, Proc. Conf. on 'Metallurgy of vacuum degassed steel products', (ed. R. Pradhan), 197-213; 1990, Warrendale, PA, TMS.
185. S. Rege, C.I. Garcia and A.J. DeArdo, in Proc. Conf. 39th Mechanical Working and Steel Processing', Indianapolis, IN, 1998, Iron and Steel Society, Vol. XXXV, 149-158.
186. Y. Tukanaga and M. Yamada, 'Method for Production of Cold Rolled Sheet Steel Having Super Deep Drawability', U.S. Patent No. 4, 504, 326.
187. R. E. Hook, in Proc. Conf. 'Metallurgy of Vacuum-Degassed Steel Products', (ed. R. Pradhan), Warrendale, PA, 1990, TMS-AIME. 263-287.
188. Luis J. Ruiz-Aparicio, C.I. Garcia and A.J. DeArdo, *Metall. Trans. A*, 2001, 32A (2), 417-423.
189. A.J. DeArdo, 'Tantalum and Niobium', 435-464; 1998, Brussels, Tantalum-Niobium International Study Center.
190. A.J. DeArdo, in Conf. Proceedings of the International Symposium on Tantalum and Niobium, Goslar, Germany, Sept. 24-28, 1995, 113-127.
191. I.A. Franson and J.D. Fritz, 'Stabilization Requirements for Type 409 (UNS S40900) Ferritic Stainless Steel', SAE Technical Paper 971005, Warrendale, PA, SAE, 1997), 155-161.
192. Y. Xu, C.I. Garcia, I. Franson, and A.J. DeArdo, in 'Low Carbon Steels for the Nineties', 397-404; Warrendale, PA, TMS-AIME.
193. A.J. DeArdo, C.I. Garcia, and J.S. Rege, in Proc. Conf. 37th MWSP Conference and International Symposium on Recovery and Recrystallization in Steel Proceedings, Hamilton, Ontario, 1996, ISS, Vol. XXXIII, 871.
194. R. G. Noonung, Jr., C. Isaac Garcia, M. Hua and A.J. DeArdo, "Role of Stabilization in Improving the Microstructure and Properties of Hot Band in Type 409 Ferritic Stainless Steels," *Stainless Steel World*, paper SSW-PO165, KCI Publishing BV, Zutphen, The Netherlands, 2001.
195. Y. Hosaya, T. Suzuki and A. Nishimoto, in "Metallurgy of vacuum degassed steel products", (ed. R. Pradhan), 291-308; 1990, Warrendale, PA, TMS.